6-1992

Double Differential Cross Sections for State-Selective Electron Capture by Low-Energy Ar^{4+} and Ar^{5+} Ions from He and Ar

Serefettin Yaltkaya
Western Michigan University

DOUBLE DIFFERENTIAL CROSS SECTIONS FOR STATE-SELECTIVE ELECTRON CAPTURE BY LOW-ENERGY Ar^{4+} AND Ar^{5+} IONS FROM He AND Ar

by

Serefettin Yaltkaya

A Thesis
Submitted to the
Faculty of The Graduate College
in partial fulfillment of the
requirements for the
Degree of Master of Arts
Department of Physics

Western Michigan University
Kalamazoo, Michigan
June 1992

DOUBLE DIFFERENTIAL CROSS SECTIONS FOR STATE-SELECTIVE ELECTRON CAPTURE BY LOW-ENERGY Ar^{4+} AND Ar^{5+} IONS FROM He AND Ar

Serefettin Yaltkaya, M.A.

Western Michigan University, 1992

Doubly differential cross sections, in angle and energy, for state-selective single-electron capture from He and Ar by Ar^{4+} and Ar^{5+} ions have been studied experimentally at laboratory impact energies of 25q, 50q, and 100q eV (q = 4 and 5, where q is the ion charge state) and at laboratory scattering angles between 0° and 5.5°, by means of translational energy spectroscopy. The translational energy-gain spectra show that only a few final states are selectively populated. Final-state transition probabilities were found to depend strongly on the charge state of the projectile ion and the ionization potential of the target atom, and only weakly on the impact energy. Multichannel Landau-Zener calculations correctly predict the positions of the dominant reaction channels that are observed and are in qualitative agreement with our measured cross sections.

ACKNOWLEDGMENTS

I have benefitted from the patience, encouragement and constructive criticism of Dr. E. Y. Kamber, my thesis advisor, without whose guidance this work would definitely not have been possible. To him, my sincere thanks must go for his invaluable help.

Next, I would like to thank the members of my committee, Dr. J. A. Tanis and Dr. R. E. Shamu for their valuable suggestions and comments offered concerning this work.

I would like to thank Dr. S. Ferguson for operating the accelerator, on which this experiment was performed, and for his valuable comments. I would also like to thank Dr. R. Haar for the many discussions concerning electronics and computers; and to thank J. A. Cornell, and J. R. Hiltbrand for building the experimental apparatus and electronic control units, respectively.

I also wish to acknowledge Anadolu University, in Turkey (Türkiye), for their support during my entire study.

Last, but certainly not least, I would like to express my deepest appreciation to my family, who continuously provided support and encouragement.

Finally, I dedicated this thesis to the memory of my grandfather, Ord. Prof. Serefettin Yaltkaya.

Serefettin Yaltkaya

Order Number 1348414

Double differential cross sections for state-selective electron capture by low-energy Ar^{4+} and Ar^{5+} ions from He and Ar

Yaltkaya, Serefettin, M.A.

Western Michigan University, 1992

U·M·I
300 N. Zeeb Rd.
Ann Arbor, MI 48106

TABLE OF CONTENTS

ACKNOWLEDGMENTS..... ii

LIST OF TABLES..... iv

LIST OF FIGURES..... v

CHAPTER

I. INTRODUCTION..... 1

II. THEORETICAL CONSIDERATIONS..... 4

Kinematics..... 5

Landau-Zener Model..... 8

Classical Over Barrier Model..... 15

Reaction Window..... 18

III. EXPERIMENTAL PROCEDURE..... 20

Recoil-Ion Production..... 20

Experimental Set-Up..... 23

IV. DATA ANALYSIS..... 30

V. RESULTS AND DISCUSSION..... 42

Ar^{4+} - He Collisions..... 42

Ar^{4+} - Ar Collisions..... 46

Ar^{5+} - He Collisions..... 50

Ar^{5+} - Ar Collisions..... 52

Kinematic Effects..... 57

CBM Model..... 60

VI. CONCLUSION..... 62

BIBLIOGRAPHY..... 64

LIST OF TABLES

1. Electron Transition Energy Levels for Ar^{4+} ($3p^2$ ^3P) - He Collisions..... 37

2. Electron Transition Energy Levels for Ar^{4+} ($3p^2$ ^3P) - Ar Collisions..... 38

3. Electron Transition Energy Levels for Ar^{5+} ($3s^2$ 3p ^2P) - He Collisions..... 40

4. Electron Transition Energy Levels for Ar^{5+} ($3s^2$ 3p ^2P) - Ar Collisions..... 41

5. Summary of Measured Collision Parameters for Single-Electron Capture Processes Compared With Classical Over Barrier Model..... 61

LIST OF FIGURES

1. Typical Charge Exchange Reaction in the Laboratory Frame..... 7

2. A Plot of the Potential Energy Curves for the Incoming and Outgoing Channels Near a Curve Crossing V(R) Versus Internuclear Separation R; - - -, Adiabatic Basis; - , Diabatic Basis..... 10

3. A Plot of Potential Curves V(R) Versus R for Multichannel States..... 14

4. Schematic Representation for Classical Potential Barrier Model for a Capture Reaction..... 16

5. Schematic Diagram of the Western Michigan University tandem Van de Graaf Accelerator Laboratory..... 21

6. Schematic Diagram of the Experimental Apparatus and the Detector Assembly..... 24

7. Electronics Block Diagram for the Translational Energy-Gain Experiment..... 27

8. Position of the Projectile Peaks as a Function of the ESA Voltages..... 29

9. A Typical Calibration Showing Channel Number Versus Voltage of the ESA Where F is the Slope (see Figure 8)..... 31

10. Energy Resolution of 250 eV Ar^{5+} Recoil Ions..... 32

11. Ar^{q+} Recoil-Ion Charge-State Intensities for 25 MeV F^{4+} Incident on Ar Gas..... 33

12. Mass-to-Charge Ratio of Ar^{q+} Recoil Projectiles as a Function of the 180°-Double Focussing Magnet Current..... 34

13. The Typical Subtraction Procedure for the Measured Energy-Gain Spectra. Channel Number is Proportional to the Q-Value..... 36

List of Figures--Continued

14. Translational Energy-Gain Spectra for Single-Electron Capture by 200 eV Ar^{4+} Ions From He at Different Scattering Angles..... 43

15. The Ratio $I(^2D)$ / $I(^2S)$ as a Function of the Scattering Angle..... 45

16. Translational Energy-Gain Spectra for Single-Electron Capture by 200 eV Ar^{4+} Ions From Ar at Different Scattering Angles..... 48

17. Differential Cross Sections for Single-Electron Capture Into the 4p State of Ar^{3+} and Transfer Ionization (TI) for 200 eV Ar^{4+} on Ar..... 49

18. Translational Energy-Gain Spectra for Single-Electron Capture by 250 eV Ar^{5+} ions From He at Different Scattering Angles..... 51

19. Probability of Single-Electron Capture as a Function of Scattering Angle for 250 eV Ar^{5+} - He Collisions..... 53

20. Translational Energy-Gain Spectra for Single-Electron Capture by 250 eV Ar^{5+} ions From Ar at Different Scattering Angles..... 55

21. Probability of Single-Electron Capture as a Function of Scattering Angle for 250 eV Ar^{5+} - He Collisions. TI Denotes Transfer Ionization..... 56

22. Translational Energy-Gain Spectra for Single-Electron Capture by Ar^{5+} Ions From Ar at Various Collision Energies..... 58

22. (a) Calculated Energy-Gain (Q) Values of (4s) and (3d) Versus Projectile Scattering Angle θ_p for Ar^{5+} - He. (b) Calculated Energy-Gain (Q) Values of (4d) and (4p) Versus Projectile Scattering Angle θ_p for Ar^{5+} - Ar..... 59

CHAPTER I

INTRODUCTION

One of the fundamental research areas in atomic physics is the study of collisions of highly charged ions with neutral target atoms. During a typical ion-atom collision three principal processes may occur: excitation, ionization, and electron capture, or a combination of these three processes. Electron capture by the projectile from the target atom (frequently called a charge transfer process) is an important process and the most probable one in low-energy collisions. In recent years, much progress has been made in the understanding of electron capture processes.

The study of electron capture by multiply-charged ions is important in the development of short-wavelength soft x-ray lasers (Lovisell, Scully, & McKnight, 1975), gas-filled radiation detectors, and both heavy-ion and electron-beam ion sources (EBIS) (Arianor & Geller, 1981). Also, this process predominates in the charge balance of the ionosphere and of interstellar clouds (Dalgarno, 1985).

The study of ion-atom collision processes is relevant for various other research areas of physics: materials science, ion accelerator technology, and, in particular, astrophysics (Butler, Heil, & Dalgarno, 1980) and astro-

physical plasmas (Pequignot, 1980). Another important application is toward the development of techniques for controlled thermonuclear fusion. For example, electron capture by fully-stripped ion impurities from deuterium atoms in a fusion plasma can lead to significant radiation cooling losses (Miller et al., 1974).

The purpose of this thesis is to investigate experimentally the process of electron capture by measuring the energy gained by Ar^{4+} and Ar^{5+} ions in collisions with Ar and He target atoms at different scattering angles and at various impact energies. Although a large number of studies have been made on state-selective single-electron capture by Ar^{4+} and Ar^{5+} ions from He and Ar, relatively little work has been reported on state-selective differential cross sections.

Previous measurements of electron capture by multiply-charged argon ions from rare-gas atoms have been reported by several investigators. Nielsen et al. (1985) measured absolute state-selective single-electron capture cross sections for 1 keV Ar^{q+} ($6 \leq q \leq 10$) ions on Ne, Ar and Xe by means of energy-gain spectroscopy. Giese et al. (1986) have used translational energy spectroscopy to determine the final-state populations following single-electron capture by Ar^{q+} ($4 \leq q \leq 8$) ions from D, D_2 and Ar at an energy of 545q eV. Puerta et al. (1985) studied single-electron capture by 200q ev Ar^{q+} ions (q=3 and 4) from rare-

gas targets. Afrosimov et al. (1986) measured the kinetic energy distributions, by using coincidence techniques, of both particles after collision of Ar^{q+} ions ($3 \leq q \leq 7$) with He. McCullough, Wilson and Gilbody, (1987) have used translational energy spectroscopy to study, at 1q keV and 2q keV, distributions of excited-product ion channels for single-electron capture by Ar^{q+} ($4 \leq q \leq 6$) ions in H, H_2 and He. Kamber (1987) has measured single and double electron capture into selected states by mean of translational energy spectroscopy for collisions of 12 keV Ar^{4+} and 15 keV Ar^{5+} with He, Ar, Kr and Ne. Very recently Biederman et al. (1990) have measured state-resolved angular distributions of single and double electron capture in 32-800 eV Ar^{6+} - Ar collisions and 19 - 200 eV Ar^{4+} - Ar collisions.

In Chapter II theoretical considerations of the electron capture process are given. Chapter III describes the production of the projectile ions, the experimental set up and the data acquisition system. In Chapter IV data analysis techniques are presented. The experimental results are presented and compared with previous studies in Chapter V. The conclusions drawn from these results are given in the last chapter.

CHAPTER II

THEORETICAL CONSIDERATIONS

In low-energy ion-atom collisions many reaction channels are possible through which electron capture may take place. The collision system may be represented by the equation

$$A^{p+}(n_o, l_o, m_o) + B \rightarrow A^{(p-q)+}(n, l, m) + B^{q+} + Q \qquad (2.1a)$$

where A is the projectile ion and B the target atom; p is the initial charge state; p-q and q are the final charge states, respectively, of A and B; Q is the energy gain; and (n_o, l_o, m_o) and (n,l,m) are the quantum numbers of the initial and final states, respectively, of the projectile ion.

There are basically three different approaches in describing the electron capture process in the low velocity region:

1. Numerical solution of the coupled channel equations with a molecular-basis expansion of the total electron wavefunction.

2. Reduction of the problem to a multichannel model which allows an analytical solution.

3. Construction of decay models of the process.

Each of these approaches has its own merits and disadvantages in describing state-selective electron capture in particular physical situations. In this chapter we shall restrict ourselves to the main ideas of the theoretical methods and shall emphasize those aspects of the theory which are directly related to the electron-capture processes of interest herein.

Kinematics

In a classical two-body collision, the translational energy of an ion undergoing an inelastic scattering process, $E_{inelastic}$, differs from the energy of the projectile ion E_o by

$$E_{inelastic} - E_o - \Delta E - \Delta K - Q \qquad (2.2)$$

where ΔK is the translational energy given to the target and ΔE is the energy defect of the reaction. The parameter Q is the total change in internal energy that takes places during the inelastic collision. This parameter is called the energy gain or loss of the collision and can be negative (endothermic reaction) or positive (exothermic reaction) depending on the binding energy of the captured electron. A typical charge exchange reaction at low collision energy in the laboratory frame of reference is

shown in Figure 1, in which the projectile ion is scattered through an angle θ_p while the recoil target ion is scattered through an angle θ_r from 90°. At low collision energies the resulting positive charge of the target normally gives rise to a small backward component of momentum for the target ion (Cooks, 1978; Giese et al., 1988). The parameter ΔE is calculated according the formula

$$\Delta E = I_p(A^{(p-q)+}) - I_p(B^{q+}) - E_j \qquad (2.3)$$

where $I_p(A^{(p-q)+})$ is the ionization potential of the projectile product ion, $I_p(B^{q+})$ is the ionization potential of the target atom after the collision, and E_j is the excitation energy of the electron after it is captured.

The translational energy ΔK given to the target is calculated according to the formula

$$\Delta K = \frac{m_p}{m_p+M}(1 - \cos\theta_p)\left[\frac{2ME_o}{m_p+M} - \Delta E\right] + \frac{m_p(\Delta E)^2}{4ME_o}\cos\theta_p \qquad (2.4)$$

where m_p is the projectile mass, M is the target mass, and E_o and θ_p are ,respectively, the initial laboratory translational energy of the projectile and the final laboratory scattering angle of the projectile (Cooks, 1978).

If the scattering angle θ_p of the projectile is close

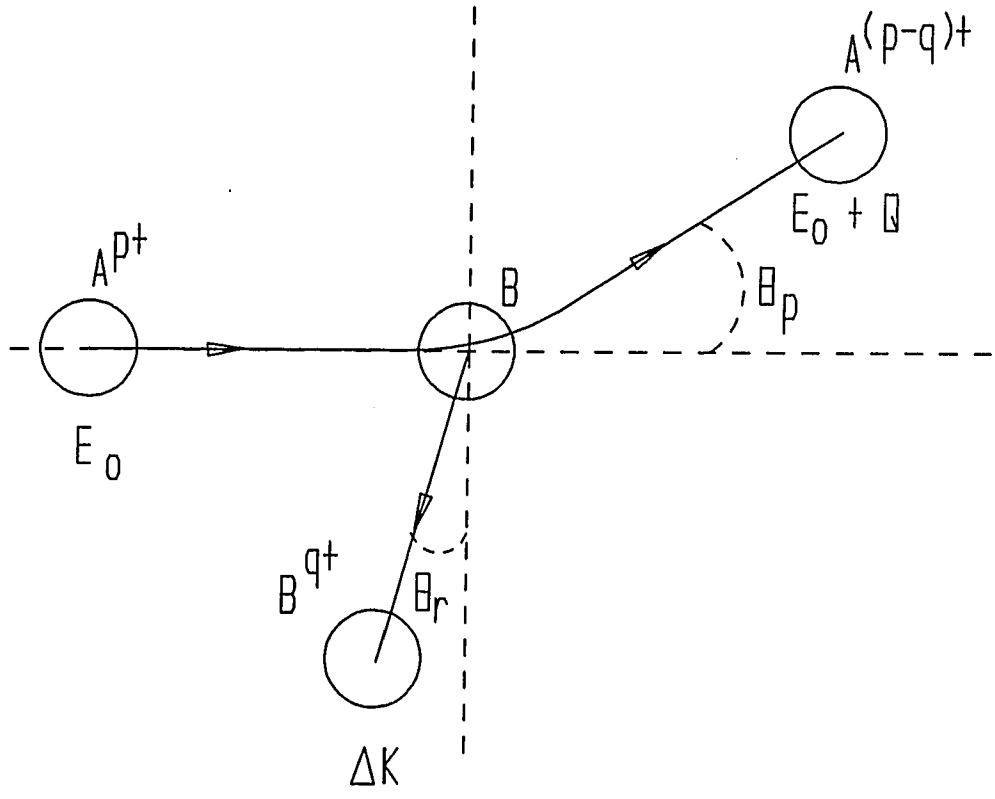

Figure 1. Typical Charge Exchange Reaction in the Laboratory Frame.

to zero, ΔK can be expressed by

$$\Delta K = \frac{m_p (\Delta E)^2}{4ME_o}. \qquad (2.5)$$

At low energies and for heavy projectile ions in collision with light targets, Kamber et al. (1987) have calculated values of ΔK for zero and non-zero scattering and found them to be large. The effect of ΔK has been observed by the same authors in O^{2+} - He collisions as a shift in the energy-gain spectrum for the ^2P capture channel at scattering angles of 0° and 2°.

Landau-Zener Model

For the process of single-electron capture by a multiply-charged ion in collision with a neutral atom, the two collision products have positive charges and the interaction between them is coulombically repulsive. Before capture, however, the ion-atom interaction is a relatively weak polarization attraction at large internuclear separations. Thus electron capture in ion-atom collisions has been recognized as a typical example of a reaction which can proceed through curve-crossing. In this model of the process the transition from initial to final state is supposed to occur near the crossing point of a pair of potential energy curves which correspond to ingoing and

outgoing channels.

The earliest theoretical work on curve-crossing was done by Landau, (1932) and Zener, (1932), who independently derived the well-known formula for the transition probability which bears their names. Stueckelberg (1932) described the motion of the nuclei semi-classically by an expansion in powers of Planck's constant and, using the extension of the JWKB method, he derived sets of connection formulas which described the effects of inelastic transitions. In this manner, Stueckelberg obtained a formula for the transition probability which included phase interference effects and which reduced in the appropriate limit to the Landau-Zener formula.

Consider the transfer of one electron from atom B to ion A of initial charge p represented by

$$A^{p+} + B \rightarrow A^{(p-1)+} + B^{+}. \qquad (2.1b)$$

In the absence of a collision interaction, the left hand and right hand members of this equation can be imagined to form two quasimolecules. Figure 2 shows the associated potential energy curves in the absence of a collision interaction between the two systems (solid curves), where the curves cross at an internuclear distance $R = R_x$. If there is a collision interaction, the potential energy curves (dashed lines) usually do not cross (an avoided

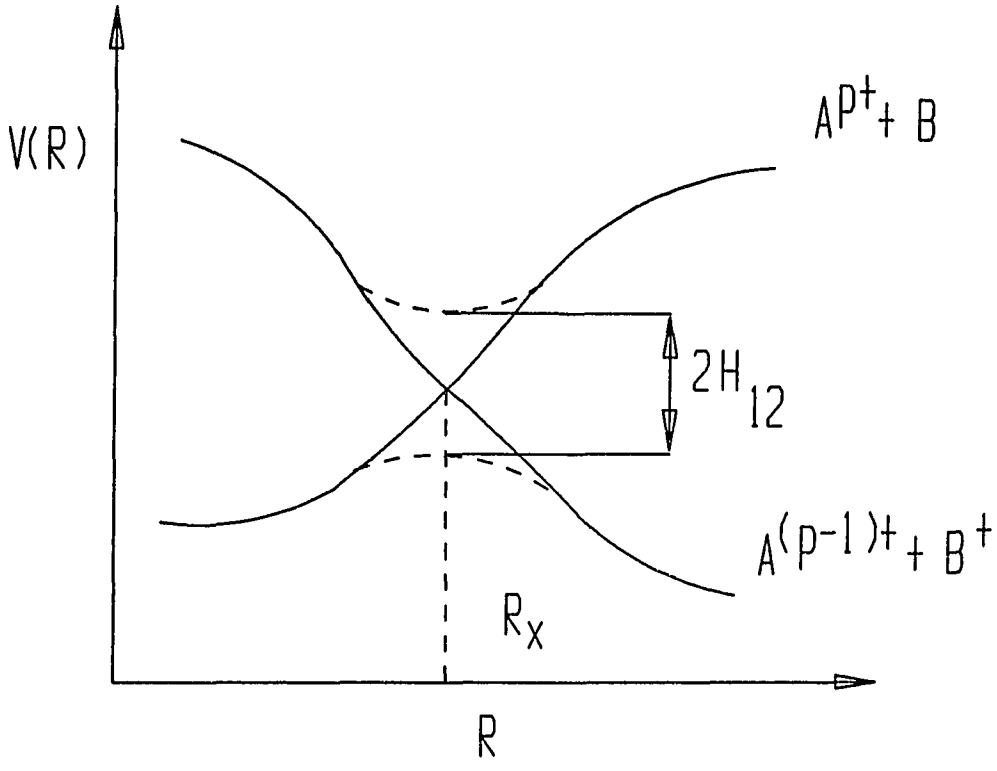

Figure 2. A Plot of the Potential Energy V(R) Curves for the Incoming and Outgoing Channels Near a Curve Crossing Versus Internuclear Separation R; - - -, Adiabatic Basis; -, Diabatic Basis.

The Coupling Matrix Element H_{12} is One-Half the Adiabatic Splitting at the Crossing Radius.

crossing) provided that the interaction matrix element is nonzero. In the region of the curve-crossing point (R_x), however, the difference in the two potential energies is small and a transition is possible, i.e., electron capture may occur.

In the Landau-Zener model, the single-crossing probability at each crossing point R_x is given by the following formula (Kimura et al., 1984)

$$P_n = \exp\left[\frac{-2\pi H_{12}^2}{v_r \Delta F}\right] \tag{2.6}$$

where H_{12} is the coupling matrix element and is approximately equal to one-half the adiabatic splitting at the curve crossing R_x (see Figure 2); and ΔF is the difference in slopes of the diabatic potential curves (solid curves) at the curve-crossing (Kimura et al., 1984). In the straight-line trajectory approximation the radial velocity v_r at the curve crossing R_x is given by

$$v_r = v_o\left[1 - \left(\frac{b}{R_x}\right)^2\right]^{\frac{1}{2}} \tag{2.7}$$

where b is the impact parameter and v_o is the relative velocity (Kimura et al, 1984). If one assumes a repulsive Coulomb interaction U_1 in the outgoing channel and zero

interaction U_2 in the incoming channel, it is possible to represent ΔF by

$$\Delta F = \frac{d}{dR}\left[U(R)_1 - U(R)_2\right]\Big|_{R=R_x} \approx \frac{q-1}{R^2} \qquad (2.8)$$

where q is the charge state of the incident ion. As always, the most difficult problem is in developing a formulation for the coupling matrix elements that can be easily applied from case to case. Olson and Salop (1976) have developed a semiempirical expression for the coupling matrix element applicable to collisions of fully-ionized ions with hydrogen atoms. Their expression is

$$H_{12}^{os} = 9.13 q^{-\frac{1}{2}} \exp\left[-1.324 \alpha R_x q^{-\frac{1}{2}}\right] \qquad (2.9)$$

where

$$\alpha = (2I_t)^{-\frac{1}{2}} \qquad (2.10)$$

and I_t is the ionization potential of the target in atomic units. Kimura et al. (1984) have reduced the coefficient of this coupling matrix element by 40%, i.e., to 5.48, in order to get good agreement with their measurements.

The probability of electron transfer for each projec-

tile curve is P = p(1-p) where p is the probability that when traversing the crossing the system remains on the same potential curve, and (1-p) is the probability for a jump from one curve to the other curve. Since there are two possible ways of traversing the potential (capture on the way in or on the way out), the total probability at a given impact parameter for two states and a single crossing (assuming that there is no interaction between the other paths and no effect associated with the rotation of the internuclear axis) is given by

$$P = 2p(1 - p). \tag{2.11}$$

The Landau-Zener formula can also be applied to multichannel states, called the multichannel Landau-Zener (MCLZ) theory, when the transition regions for each channel are well separated. The general expression for N states and N-1 crossings is given by Salop and Olson (1975), assuming that there is no interference between different paths leading to a particular final state (see Figure 3). The probability for capture into the nth final state is

$$\begin{aligned} P_n = {} & p_1 p_2 \ldots p_n (1 - p_n) \left[1 + (p_{n+1} p_{n+2} \ldots p_N)^2 + \right. \\ & (p_{n+1} p_{n+2} \ldots p_{N-1})^2 (1 - p_n)^2 + (p_{n+1} p_{N-2})^2 + \\ & \left. (1 - p_{N-1})^2 + \ldots + p_{n+1}^2 (1 - p_{n+2})^2 + (1 - p_{n+1})^2 \right]. \end{aligned} \tag{2.12}$$

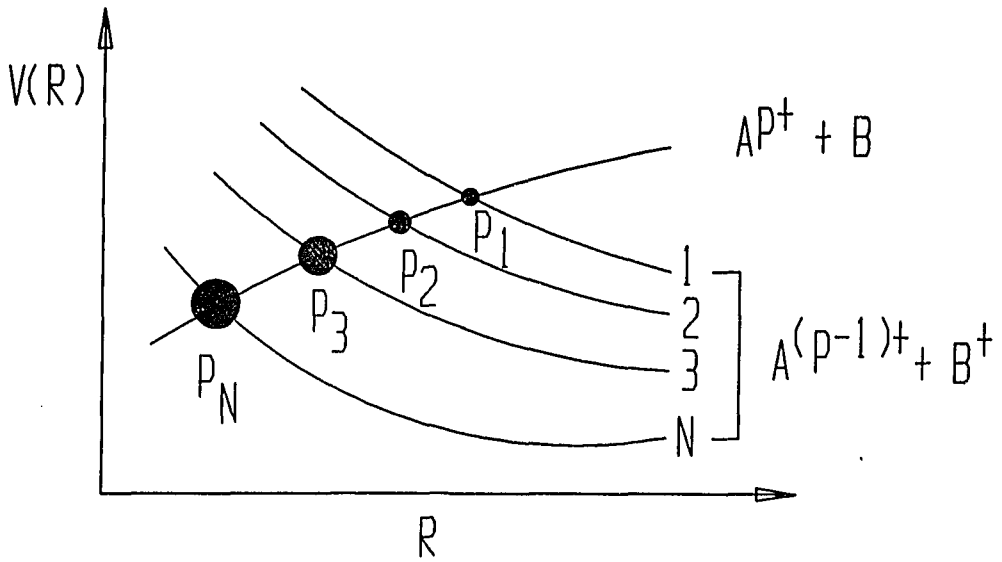

Figure 3. A Plot of Potential Curves V(R) Versus R for Multichannel States.

For the case of partially-stripped projectiles, Taulbjerg (1986) has suggested a correction term to H_{12}. This correction term depends on the quantum numbers n and ℓ of the state into which the transferred electron is captured and is given by

$$f_{nl} = \frac{(-1)^{n+l-1}(2l+1)^{\frac{1}{2}}\Gamma(n)}{[\,\Gamma(n+l+1)\Gamma(n-1)\,]^{\frac{1}{2}}}. \qquad (2.13)$$

The coupling matrix element is thus

$$H_{12}^{os} = f_{nl} 9.13 q^{-\frac{1}{2}} \exp[-1.324 \alpha R_x q^{-\frac{1}{2}}]. \qquad (2.14)$$

The cross section (σ_n) for capture into a particular final state n is given in terms of the impact parameter b and crossing distance R_x by

$$\sigma_n = 2\pi \int_0^{R_x} P_n b db \qquad (2.15)$$

where P_n is the probability for capture into the nth final state.

Classical Over Barrier Model

The classical over barrier transition model (CBM), originally proposed by Bohr and Lindhard (1954), has been used for a qualitative explanation of the main features of the electron capture process by Ryufuku et al. (1980) and Mann et al. (1981). This model describes a projectile ion of charge q approaching a target atom and creating a potential barrier as shown in Figure 4.

The electron will be transferred when it has enough energy to overcome the potential barrier between the collision partners. This barrier is given by the superposition of the two Coulomb potentials

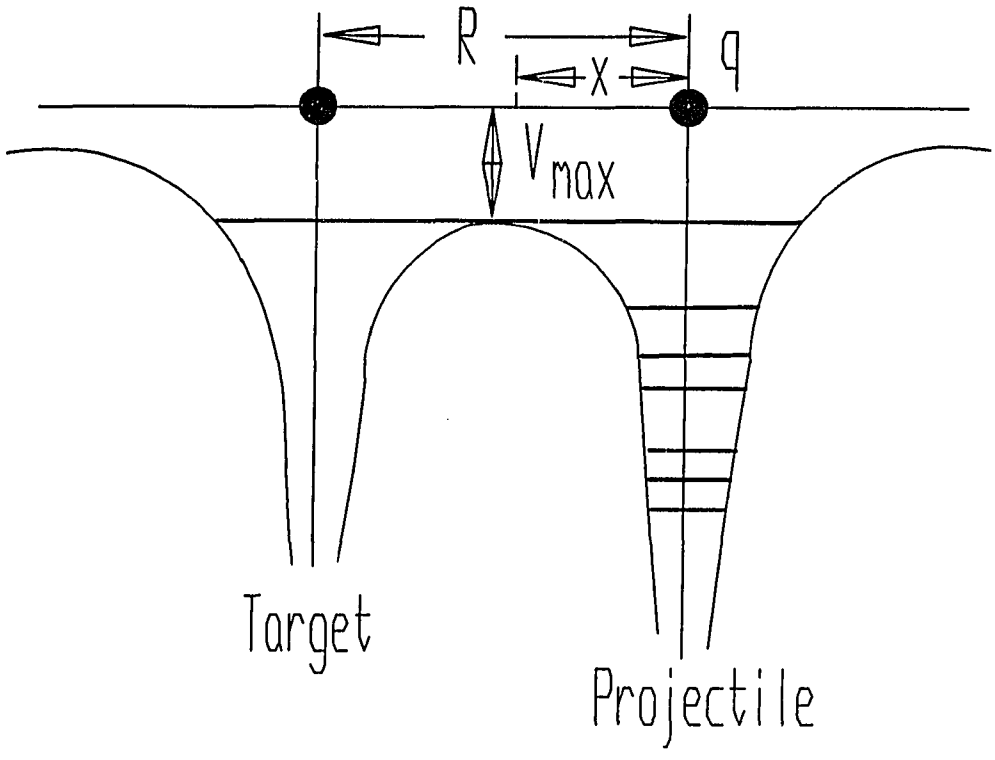

Figure 4. Schematic Representation of Classical Potential Over Barrier Model for a Capture Reaction.

$$V(x) = -\frac{q}{x} - \frac{1}{R-x} \qquad (2.16)$$

where R is the internuclear distance and x is the distance measured along the internuclear axis between the electron and the projectile (see Figure 4). Electron transfer takes places if two conditions are met. The first condition is

$$-I_t - \frac{q}{R} = -\frac{q^2}{2n^2} - \frac{1}{R} \qquad (2.17)$$

where on the left the first term is the ionization potential of the electron when bound to the target atom and the second term is the Coulomb energy due to the projectile ion, while on the right side the first term is the energy of the electron when bound to a level of quantum number n of the projectile and the second term is the coulomb energy due to the singly-ionized target atom. The second condition for electron transfer is

$$-I_t - \frac{q}{R} \geq V_{max} \qquad (2.18)$$

that is, the energy of the bound electron in the Coulomb field of the projectile ion must be equal to or greater than the maximum barrier height V_{max}, where V_{max} can be shown from Equation (2.16) to be

$$V_{max} = -\frac{(\sqrt{q}+1)^2}{R}. \qquad (2.19)$$

One can solve Equations 2.17 - 2.19 to find the critical internuclear distance at which the electron transfer occurs and determine the effective principal quantum

number n_{cbm} which is populated by the electron capture process (Mann, Folkmann, & Beyer, 1981; Ryufuku, Sasaki, & Watanabe, 1980,).

$$R_{cbm} \leq \frac{2\sqrt{q}+1}{I_t} \tag{2.20}$$

$$n_{cbm} = q(2I_t[\frac{1+(q-1)}{2\sqrt{q}+1}])^{-\frac{1}{2}}. \tag{2.21}$$

Reaction Window

The important curve crossings between the diabatic potential energy curves (see Figure 2) associated with the entrance channel and various exit channels are those which occur at moderate internuclear separations, where the probability for single-electron capture is large. This intermediate range of separations is commonly referred to as the reaction window for the electron capture process. The position of the reaction window for any collision system depends mainly on the collision energy of the projectile. When the collision energy is reduced the adiabaticity at inner crossings becomes increasingly pronounced, while the transition probability at distant crossings becomes larger. Therefore, the reaction window shifts toward larger inter-

nuclear separations if the collision energy is reduced and vice versa. Several authors have calculated the location of the reaction window as a function of the crossing radius. (Cederquist et al., 1985; Kimura et al., 1984; Meyer et al., 1985; Niehaus, 1985; Taulbjerg, 1986).

CHAPTER III

EXPERIMENTAL PROCEDURE

In this work a fast fluorine beam from the Western Michigan University (WMU) tandem Van de Graaff Accelerator was used to "pump" a recoil-ion source. The fluorine beam was focussed on argon or helium target gas, resulting in the production of recoil ions which were subsequently used as secondary projectile ions. A general layout of the WMU accelerator laboratory is shown in Figure 5.

Recoil-Ion Production

The beginning point of the fluorine beam is the source of negative ions by cesium sputtering (SNICS). In the SNICS ionized cesium atoms, heated by a tungsten coil, sputter fluorine atoms from a calcium fluoride (CaF_2) cathode. The sputtered fluorine ions capture electrons due to collisions with the cesium atoms in the close vicinity of the cathode, thereby becoming negative ions. These negative ions are repelled by the cathode and accelerated through the extraction electrode and the focus electrodes located in the SNICS. The negative ion beam then passes through a 20° inflection magnet that allows selection of the desired ion species, i.e., F^-, and bends this beam into the accelerator

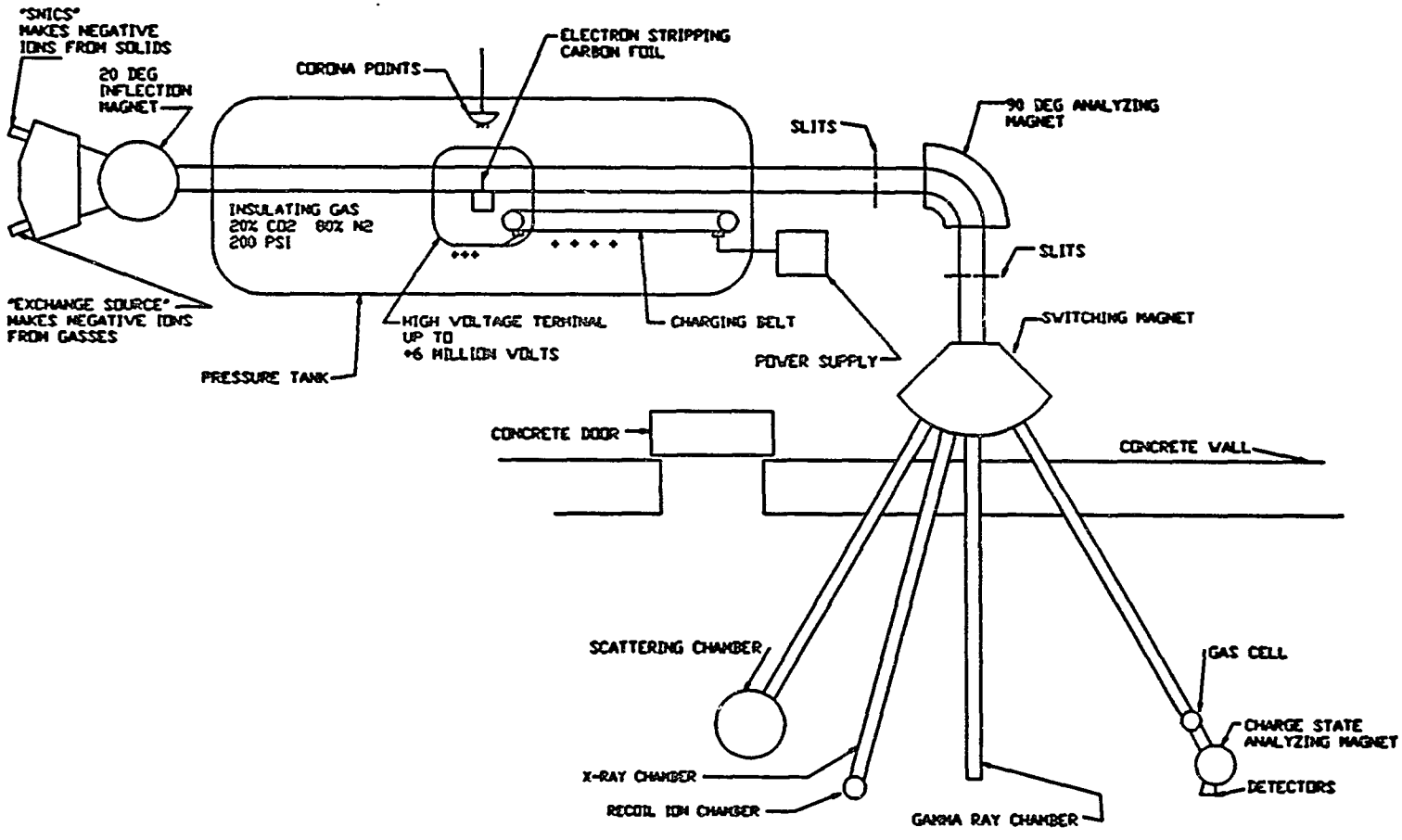

Figure 5. Schematic Diagram of the Western Michigan University Tandem Van de Graaff Accelerator Laboratory.

beam line. Adjustment of the position of the beam is accomplished using electrostatic steerers and the beam is focussed by an einzel lens before entering the low energy end of the accelerator.

Negative ions are accelerated toward the positively charged (up to +6 million volts) high voltage terminal in the center of the accelerator and pass through a gas stripper where electrons are removed from the ions so that the ions become positively charged. These positively charged ions are then repelled by the terminal and accelerated out of the high-energy end of the accelerator. The accelerator tank contains insulating gas consisting of a mixture of 20% CO_2 and 80% N_2 at 200 psi. The accelerated beam then passes through a high-energy quadrupole magnet and some defining slits.

The beam emerging from the accelerator consists of several charge states of different beam energies which are analyzed by a 90°-analyzing magnet in order to select the desired charge state and energy. The field in the 90°-analyzing magnet is measured by a nuclear magnetic resonance (NMR) technique. The 90°-analyzing magnet focusses the beam on a set of image slits. The portion of the beam striking the image slits produces a current imbalance on the slits due to energy fluctuations in the beam. This current difference between the two image slits can then be fed back to the terminal corona system to stabilize the

terminal high voltage. To select among several beam lines set up for different experiments in the target room a switching magnet is used.

Experimental Set-Up

A schematic diagram of the recoil-ion experimental apparatus is shown in Figure 6. The pump beam is post-stripped to a median charge state of 7+ by using a carbon foil and then collimated by four-jaw slits before entering the recoil-ion source where highly charged argon projectile ions were produced. The recoil-ion source consists of a semispherical electrode with voltage V_1 and a flat plate electrode with voltage V_2, and has 3 mm diameter entrance and exit apertures where the pump beam passes through. After the pump beam passes through the interaction region in the recoil-ion source, it is collected by a Faraday cup (FC). The gas pressure in the recoil ion source ($\sim 1\times10^{-3}$ Torr) is adjusted until the background pressure in the main chamber increases from $\sim 2\times10^{-6}$ Torr to $\sim 3\times10^{-6}$ Torr. Recoil ions were extracted perpendicular to the pump beam with acceleration voltage V_{acc} (Giese et al., 1986):

$$V_{acc} = V_2 + 0.75(V_1 - V_2) \qquad (3.1)$$

In the present experiment (V_1-V_2) was always less than 2 volts. A pair of deflection plates (D_1) is used to focus

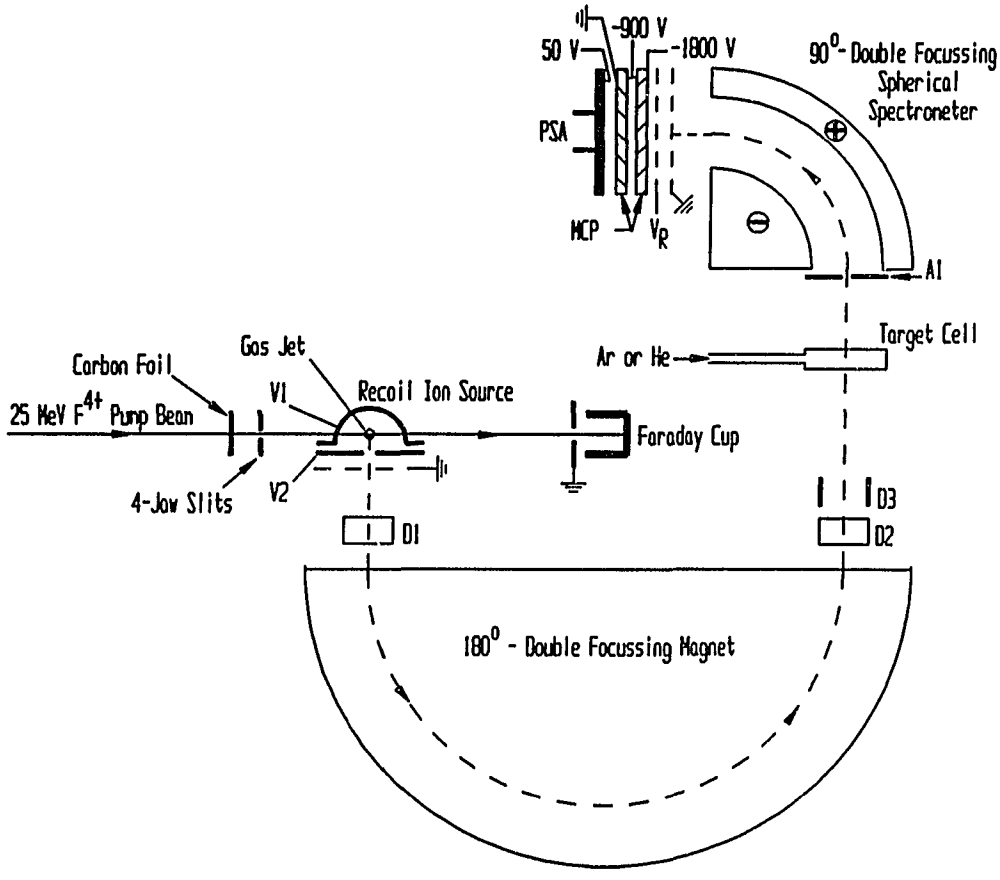

Figure 6. Schematic Diagram of the Experimental Apparatus and the Detector Assembly.

and steer the beam extracted from the recoil-ion source into a 180°-double focussing magnetic spectrometer. After charge analysis, the recoil ion beam was focused on a 3 mm long target cell by another pair of deflection plates (D2 and D3). The entrance and exit apertures of the target cell are 1 mm and 2mm, respectively. The target gas pressure in the collision cell was sufficiently low (~1x10^{-6} Torr) to ensure single collision conditions.

Scattered ions emerging from the target cell which undergo electron capture were energy analyzed by a 90°-double focussing electrostatic analyzer (ESA) at a particular scattering angle. The scattering angle is selected by means of an aperture A1 (1 mm diameter). The mean radius of the ESA is 35 mm. The energy E of a scattered ion of charge q passing through the ESA is given by,

$$E = qV_{acc} = qkV \qquad (3.2)$$

where q is the atomic charge, k is the ESA constant (k=2.3 for this ESA) and V is the voltage applied to the ESA (Kamber et al., 1987). The analyzed ions were detected by a one-dimensional position-sensitive microchannel plate detector. The detector device consists of two 3.25 cm diameter microchannel plates (MCP) and a position-sensitive anode (PSA).

The detector operates in the following manner. When

an ion strikes the front channel plate the resulting electron cascade from the two microchannel plates is collected by the anode. The fraction of charge collected on electrodes located at each side of the anode is inversely proportional to the distance from the electrode where the electrons hit the anode (see Figure 7). The relative position of the ions striking the MCP is then determined by the ratio between the resulting voltage pulse at one electrode and the sum of the voltage pulses of the two electrodes, that is

$$X = \frac{V_U}{(V_U + V_L)} \qquad (3.3)$$

where X is the relative position along the active dimension, V_U is the voltage of the upper electrode, and V_L is the voltage of the lower electrode.

Data were collected using the electronics set up shown schematically in Figure 7. Signals from each electrode of the position sensitive anode (PSA) were first identically amplified by using pre-amplifiers (Ortec model 109A) and spectroscopy amplifiers (AMP, Ortec model 451) and then summed using a dual sum/invert amplifier (DSI, Tennelec model TC253). The signal then passed to the position sensitive detector analyzer (PSD Analyzer, Ortec model 466) where the voltage signals were divided, producing a voltage

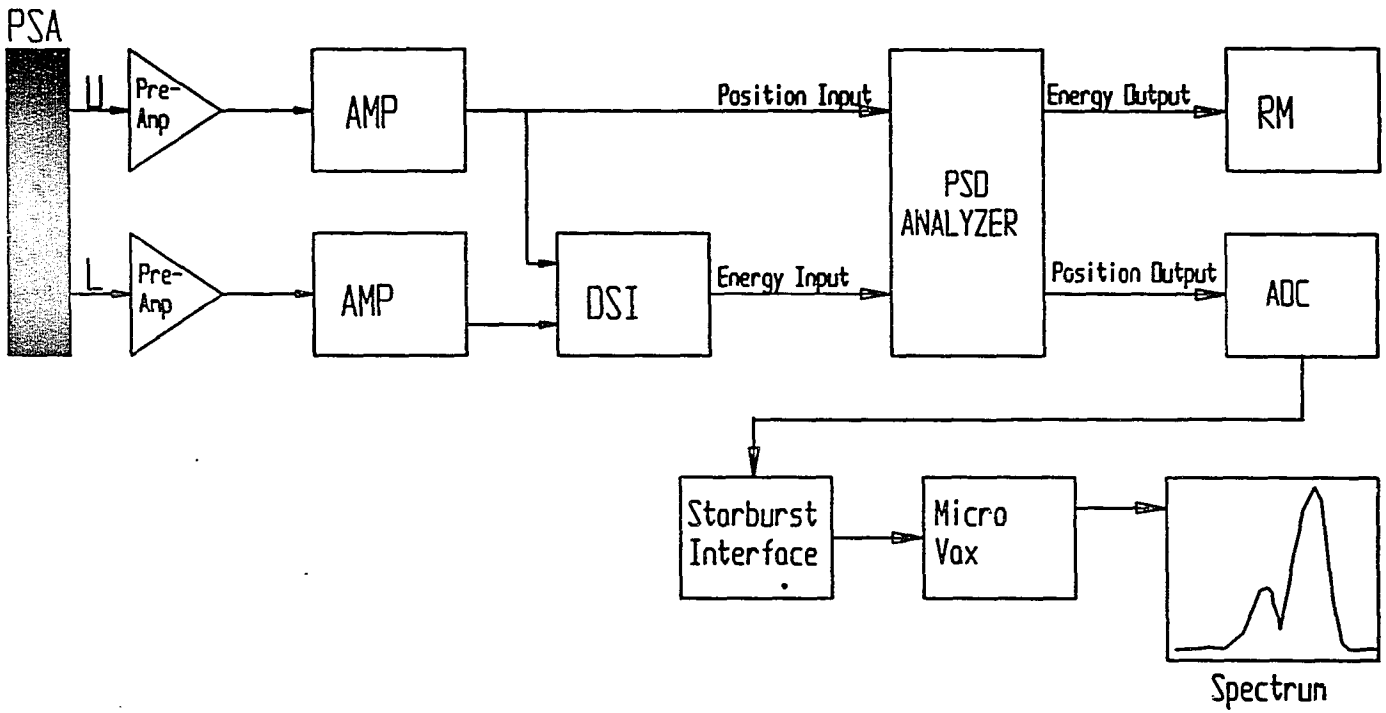

Figure 7. Electronics Block Diagram for the Translational Energy-Gain Experiment.

U and L are the Upper and Lower Electrodes of the Position Sensitive Detector Anode (PSA), Respectively.
DSI = Dual Sum/Invert Amplifier. RM = Ratemeter.
PSD = Position Sensitive Detector. ADC = Analog-to-Digital Converter.

signal whose height was proportional to the location of the incident ion's position and routed to an analog-to-digital converter (ADC). The pulse rate of the output signal (Energy output) was measured using a ratemeter (RM, Ortec model 744).

A STARBURST interface module was used to transfer data to a MicroVAX computer system enabling conversion from position distribution information to energy distribution information. In order to minimize distortion due to small changes in linearity near the edges of the MCP, only the central portion of the microchannel plates was used.

The detector was periodically calibrated by positioning the direct beam at different locations and then varying the applied voltage to the ESA. Spectra were recorded at each voltage in order to generate a calibration curve (see Figure 8).

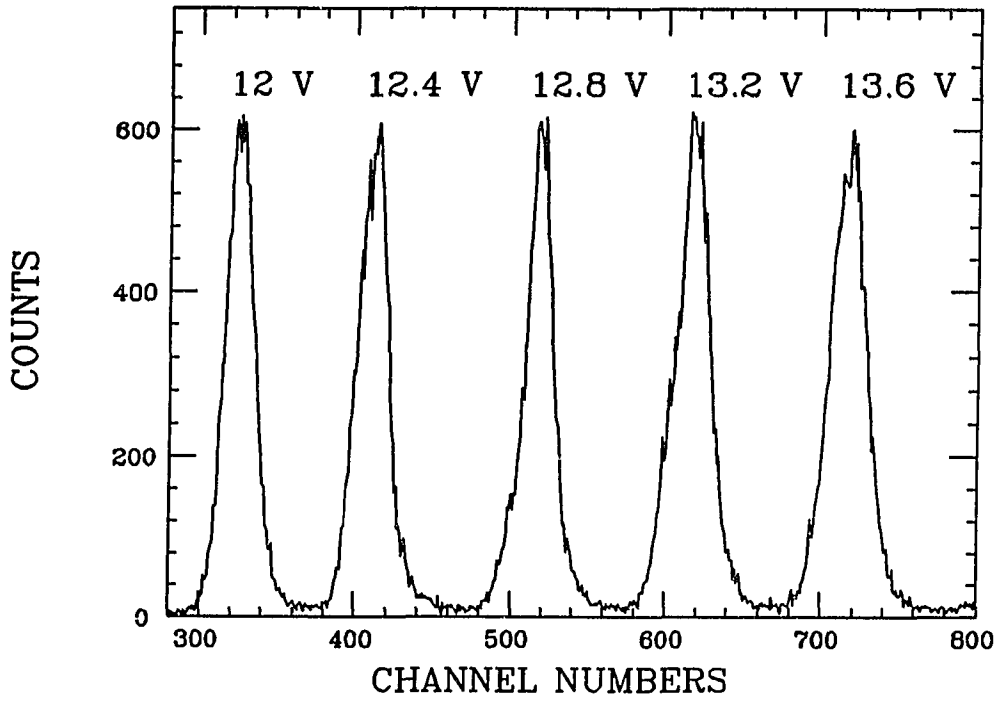

Figure 8. Position of the Projectile Peaks as a Function of the ESA Voltages.

CHAPTER IV

DATA ANALYSIS

In the first part of the experiment, the position distribution of the scattered ions following single electron capture was measured, with the voltage applied to the ESA given by

$$V = \frac{qV_o}{q'} \tag{4.1}$$

where q and q' are the charge states of the projectile before and after the collision, respectively, and V_0 is the voltage applied to the ESA for which the direct beam is passed.

The energy gain Q corresponding to V_{acc} (see Equation 3.1) is given by (Kamber et al., 1987)

$$Q = \left[\left(\frac{q'V}{qV_o}\right) - 1\right] V_{acc} q. \tag{3.4}$$

The energy gain in terms of the position of the projectile peak is

$$Q(x) = \left[\frac{(S(0) - S(x))}{(FV_o - S(0) + S(x))}\right] V_{acc} q \qquad (4.3)$$

where S(0) and S(x) are the positions of the main peaks of the uncharge-changed projectiles and the charge-changed product ions, respectively, and F is the slope of the position of the projectile peak as a function of ESA voltage (see Figure 9) (Kamber et al., 1987). The energy

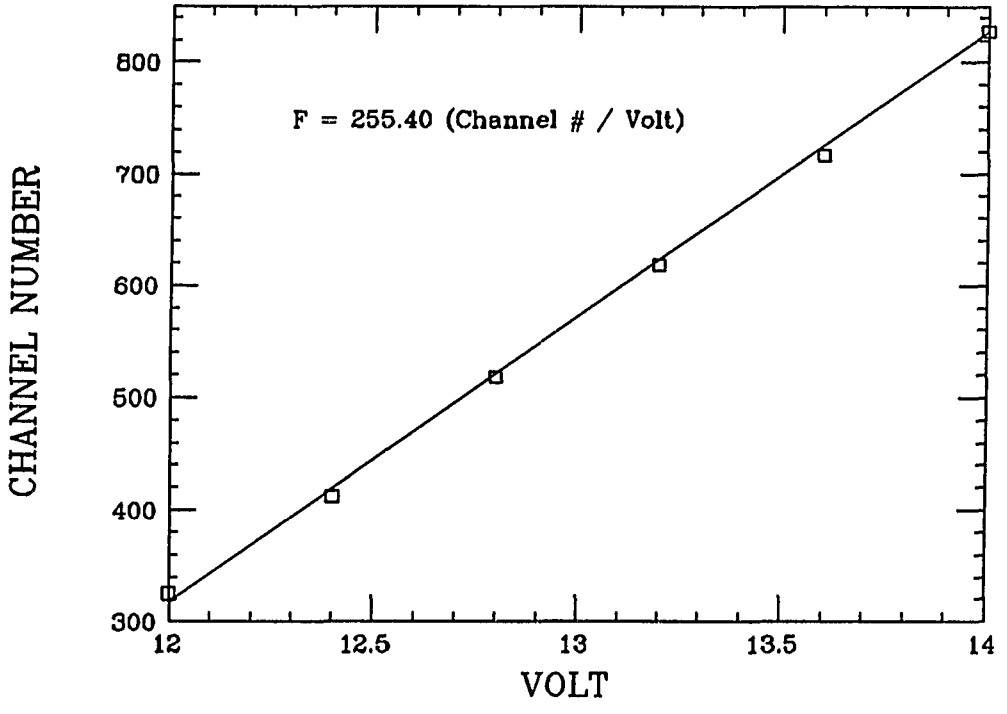

Figure 9. A Typical Calibration Showing Channel Number Versus Voltage of the ESA Where F is the Slope (see Figure 8).

resolution of the ESA for a 250 eV Ar^{5+} projectile beam (produced from recoil ions) was found to be 1.65 eV at full

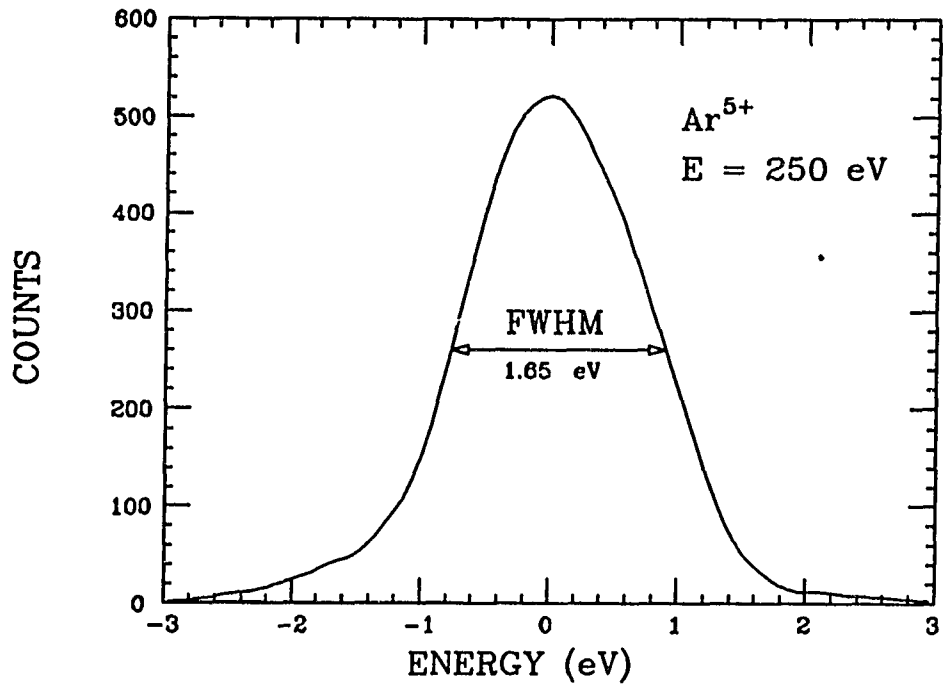

Figure 10. Energy Resolution of 250 eV Ar^{5+} Recoil Ions.

width half maximum (FWHM) as shown in Figure 10.

A charge-state spectrum of argon recoil ions produced in the recoil-ion source was obtained by varying the magnet current of the 180°-double focussing magnet. Figure 11 shows Ar^{q+} recoil ions with charge states ranging from 1+ to 8+ obtained with intensities sufficient for the energy gain measurements. To identify the charge state of each peak, we plotted the square root of the mass-to-charge ratio (assuming the mass of argon for each peak) of the recoil ion peaks in Figure 11 as a function of the 180°-double focussing magnet current. The results are plotted in

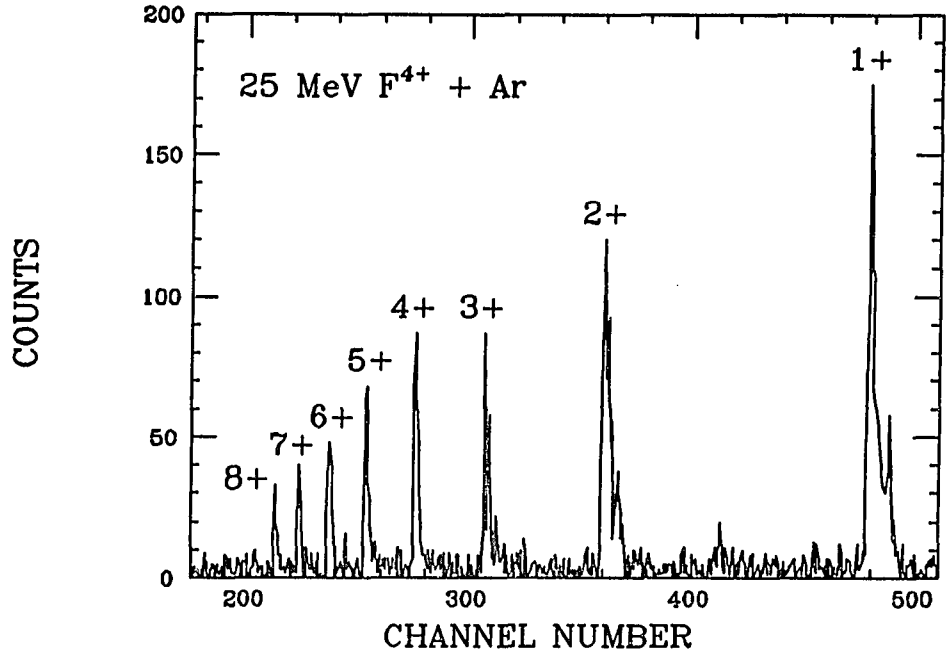

Figure 11. Ar^{q+} Recoil-Ion Charge-State Intensities for 25 MeV F^{4+} Incident on Ar Gas.

Figure 12 (the channel numbers were converted to current of the 180°-double focussing magnet).

A typical energy-gain spectrum for electron capture is shown in Figure 13a for 250 eV Ar^{5+} + Ar. In order to determine contributions from the background gas, the experiment was repeated without gas in the target cell. After normalizing each run to the total amount of pump beam charge collected, the background runs were subtracted from the runs with target gas to produce a spectrum corresponding to the energy distribution of Ar^{5+} ions capturing a single electron from Ar (see Figure 13).

For the different collision systems investigated the

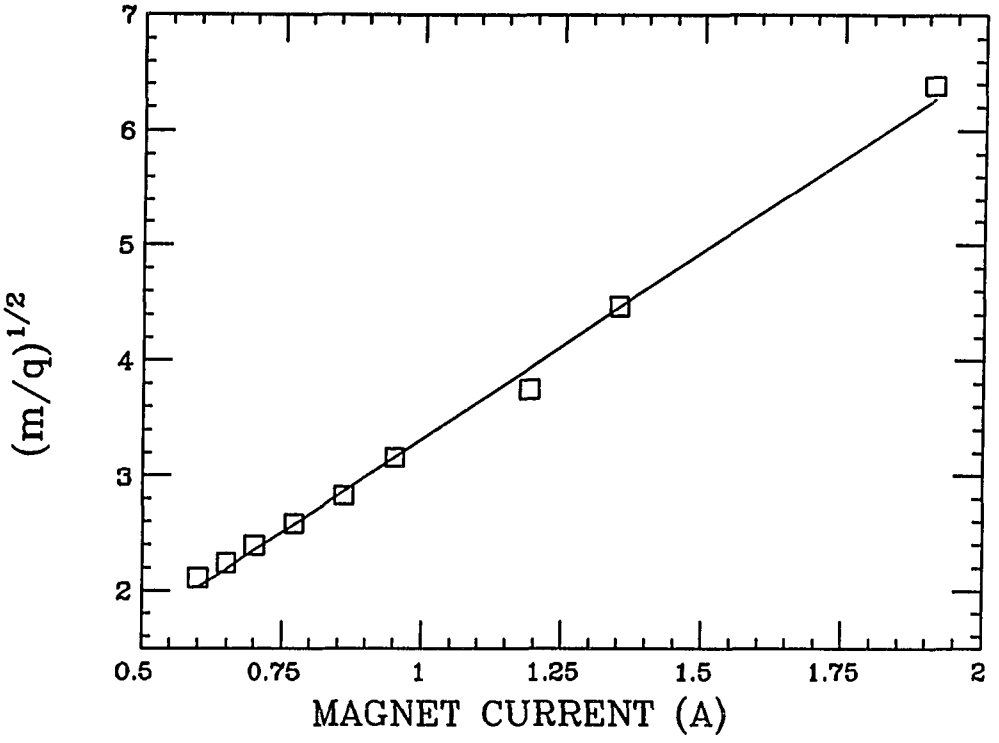

Figure 12. The Mass-to-Charge Ratio of Ar^{q+} Recoil Projectiles as a Function of the 180° -Double Focussing Magnet Current.

possible outgoing channels following single-electron capture are listed in Tables 1-4. The ionic energy levels used in preparing these tables were taken from Bashkin and Stoner (1978). These tables were used to determine which outgoing reaction channels are observed in the collision processes studied here.

Errors in the measured Q-values are mainly due to the least-squares fit to the calibration curve (± 2%) and the stability of the voltage applied to the ESA (± 1%). Under these conditions errors in the translational energy scale,

as calibrated against the scattered ions, were always less than ±1 eV.

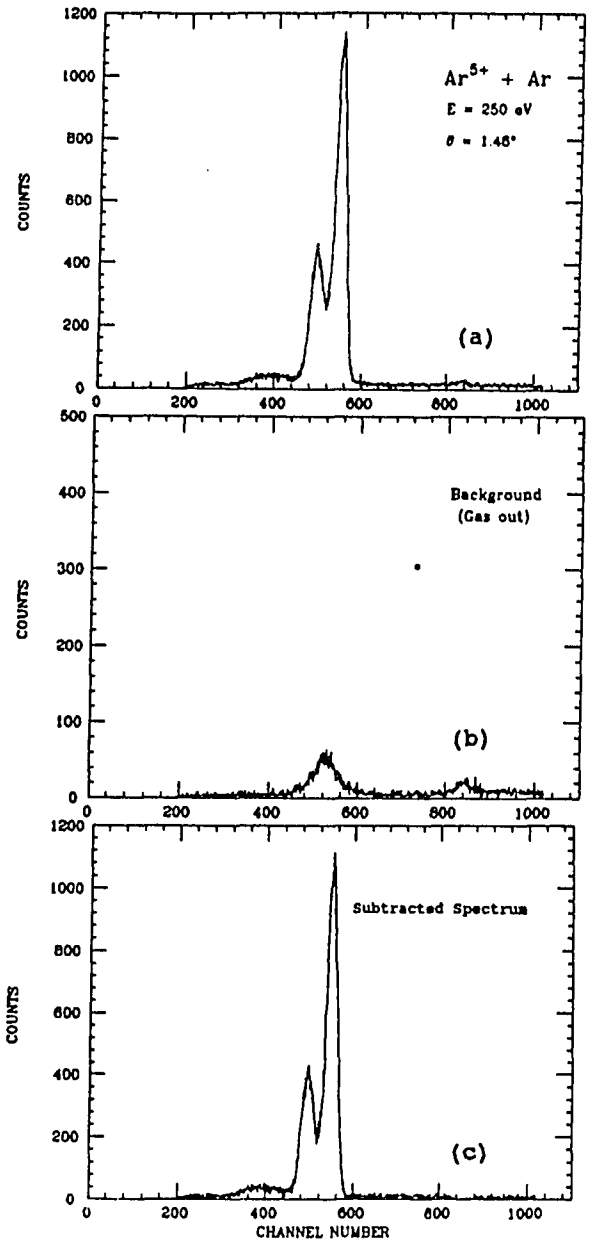

Figure 13. Typical Subtraction Procedure for the Measured Energy-Gain Spectra. Channel Number is Proportional to the Q-Value.

Spectrum (a) = Single-Electron Capture by 250 eV Ar^{5+} Ions From Ar and Background Gas.
Spectrum (b) = Single-Electron Capture by 250 eV Ar^{5+} Ions From Background Gas.
Spectrum (c) = Spectrum (a) - Spectrum (b).

Table 1

Electron Transition Energy Levels for Ar^{4+} ($3p^2\ ^3P$) - He Collisions

Projectile Product	Energy Defect ΔE(eV)
Ar^{3+} ($3s^2\ 3p^3\ ^2D$)	+ 32.60
Ar^{3+} ($3s^2\ 3p^3\ ^2P$)	+ 30.89
Ar^{3+} ($3s\ 3p^4\ ^4P$)	+ 20.47
Ar^{3+} ($3s\ 3p^4\ ^2D$)	+ 17.13
Ar^{3+} ($3s\ 3p^4\ ^2P$)	+ 14.47
Ar^{3+} ($3s\ 3p^4\ ^2S$)	+ 13.19
Ar^{3+} ($3p^2\ 3d\ ^4P$)	+ 7.78
Ar^{3+} ($3p^2\ 3d\ ^2P$)	+ 7.50

Source: Bashkin, S., & Stoner, J.O. (1978). Atomic energy levels and Grotrian Diagrams (Amsterdam: North-Holland, 239-241).

Table 2

Electron Transition Energy Levels for
Ar^{4+} ($3p^2\ ^3P$) - Ar Collisions

Projectile Product	Energy Defect ΔE(eV)
Ar^{3+} ($3s^2\ 3p^3\ ^2D$)	+ 41.42
Ar^{3+} ($3s^2\ 3p^3\ ^2P$)	+ 39.71
Ar^{3+} ($3s\ 3p^4\ ^4P$)	+ 29.29
Ar^{3+} ($3s\ 3p^4\ ^2D$)	+ 25.95
Ar^{3+} ($3s\ 3p^4\ ^2P$)	+ 23.29
Ar^{3+} ($3s\ 3p^4\ ^2S$)	+ 22.01
Ar^{3+} ($3p^2\ 3d\ ^4P$)	+ 16.60
Ar^{3+} ($3p^2\ 3d\ ^2P$)	+ 16.32
Ar^{3+} ($3p^2\ 3d'\ ^2D$)	+ 14.33
Ar^{3+} ($3p^2\ 3d'\ ^2F$)	+ 13.45
Ar^{3+} ($3p^2\ 3d'\ ^2P$)	+ 13.43
Ar^{3+} ($3p^2\ 3d'\ ^2P$)	+ 12.93
Ar^{3+} ($3s^2\ 3p^2\ (^3P)\ 4s\ ^4P$)	+ 12.81
Ar^{3+} ($3s^2\ 3p^2\ (^3P)\ 4s\ ^2P$)	+ 12.14
Ar^{3+} ($3s^2\ 3p^2\ (^3D)\ 4s\ ^2D$)	+ 10.80
Ar^{3+} ($3s^2\ 3p^2\ (^3P)\ 4p\ ^4D$)	+ 8.40
Ar^{3+} ($3s^2\ 3p^2\ (^3P)\ 4p\ ^4P$)	+ 8.12
Ar^{3+} ($3s^2\ 3p^2\ (^3P)\ 4p\ ^2D$)	+ 7.89
Ar^{3+} ($3s^2\ 3p^2\ (^3P)\ 4p\ ^4S$)	+ 7.88
Ar^{3+} ($3s^2\ 3p^2\ (^3P)\ 4p\ ^2P$)	+ 7.37

Table 2--Continued

Projectile Product	Energy Defect ΔE(eV)
Ar^{3+} $(3s^2\ 3p^2\ (^3P)\ 4p\ ^2S)$	+ 6.91
Ar^{3+} $(3s^2\ 3p^2\ (^3P)\ 4p'\ ^2F)$	+ 6.31
Ar^{3+} $(3s^2\ 3p^2\ (^1D)\ 4p'\ ^2D)$	+ 6.07

Source: Bashkin, S., & Stoner, J.O. (1978). Atomic energy levels and Grotrian Diagrams (Amsterdam: North-Holland, 239-241).

Table 3

Electron Transition Energy Levels for $Ar^{5+}(3s^2\ 3p\ ^2P)$- He Collisions

Projectile Product	Energy Defect ΔE(eV)
Ar^{4+} $(3S^2\ 3p\ (^2P)\ 3d\ ^3P)$	+ 23.32
Ar^{4+} $(3S^2\ 3p\ (^2P)\ 3d\ ^3D)$	+ 22.55
Ar^{4+} $(3S^2\ 3p\ (^2P)\ 3d\ ^1F)$	+ 20.01
Ar^{4+} $(3S^2\ 3p\ (^2P)\ 3d\ ^1P)$	+ 19.17
Ar^{4+} $(3s^2\ 3p\ (^2P)\ 4s\ ^3P)$	+ 13.50
Ar^{4+} $(3s^2\ 3p\ (^2P)\ 4s\ ^1P)$	+ 13.07
Ar^{4+} $(3s^2\ 3p\ 4p\ ^1P)$	+ 8.81
Ar^{4+} $(3s^2\ 3p\ 4p\ ^3D)$	+ 8.49
Ar^{4+} $(3s^2\ 3p\ 4p\ ^3D)$	+ 8.42
Ar^{4+} $(3s^2\ 3p\ 4p\ ^3D)$	+ 8.25
Ar^{4+} $(3s^2\ 3p\ 4p\ ^3S)$	+ 7.78
Ar^{4+} $(3s^2\ 3p\ 4p\ ^3P)$	+ 7.74
Ar^{4+} $(3s^2\ 3p\ 4p\ ^3P)$	+ 7.62
Ar^{4+} $(3s^2\ 3p\ 4p\ ^3P)$	+ 7.57
Ar^{4+} $(3s^2\ 3p\ 4p\ ^1D)$	+ 6.81
Ar^{4+} $(3s^2\ 3p\ 4p\ ^1S)$	+ 5.61

Source: Bashkin, S., & Stoner, J.O. (1978). Atomic energy levels and Grotrian Diagrams (Amsterdam: North-Holland, 243-245).

Table 4

Electron Transition Energy Levels for $Ar^{5+}(3s^2\ 3p\ ^2P)$- Ar Collisions

Projectile Product	Energy Defect ΔE(eV)
Ar^{4+} $(3s^2\ 3p\ 4p\ ^1P)$	+ 17.65
Ar^{4+} $(3s^2\ 3p\ 4p\ ^3D)$	+ 17.32
Ar^{4+} $(3s^2\ 3p\ 4p\ ^3D)$	+ 17.25
Ar^{4+} $(3s^2\ 3p\ 4p\ ^3D)$	+ 17.08
Ar^{4+} $(3s^2\ 3p\ 4p\ ^3S)$	+ 16.61
Ar^{4+} $(3s^2\ 3p\ 4p\ ^3P)$	+ 16.57
Ar^{4+} $(3s^2\ 3p\ 4p\ ^3P)$	+ 16.45
Ar^{4+} $(3s^2\ 3p\ 4p\ ^3P)$	+ 16.40
Ar^{4+} $(3s^2\ 3p\ 4p\ ^1D)$	+ 15.64
Ar^{4+} $(3s^2\ 3p\ 4p\ ^1S)$	+ 14.48
Ar^{4+} $(3s^2\ 3p\ 4d\ ^1D)$	+ 10.10
Ar^{4+} $(3s^2\ 3p\ 4d\ ^3F)$	+ 9.98
Ar^{4+} $(3s^2\ 3p\ 4d\ ^3D)$	+ 9.70
Ar^{4+} $(3s^2\ 3p\ 4d\ ^3P)$	+ 9.31
Ar^{4+} $(3s^2\ 3p\ 4d\ ^1P)$	+ 8.69

Source: Bashkin, S., & Stoner, J.O. (1978). Atomic energy levels and Grotrian Diagrams (Amsterdam: North-Holland, 243-245).

CHAPTER V

RESULTS AND DISCUSSION

In this chapter the experimental results and discussion of individual collision systems are presented.

Ar^{4+} - He Collisions

Figure 14 shows the translational energy-gain spectra obtained for single electron capture by 200 eV Ar^{4+} ions from He at different scattering angles. Also shown are reaction windows calculated on the basis of a single crossing Landau-Zener theory using two values of H_{12}. The vertical lines show the results of multichannel Landau-Zener (MCLZ) calculations. At 0° scattering angle, two peaks are clearly resolved and seen. The dominant peak correlates with capture from incident ground state Ar^{4+} ($3p^2$ ^3P) ions into the excited state ($3p^4$ ^2S) of the Ar^{3+} ion (see Table 1), in agreement with previous measurements at higher energies and forward scattering angles (Afrosimov et al., 1986; Kamber, 1988; McCullough et al., 1987; Puerta et al., 1985). This process is exothermic by 12.5 eV. There are also significant contributions from capture into the $3p^4$ ^2P state. The peak at Q ≈ 15 eV arises from capture into the $3p^4$ ^2D state of Ar^{3+}. It is expected that the inci-

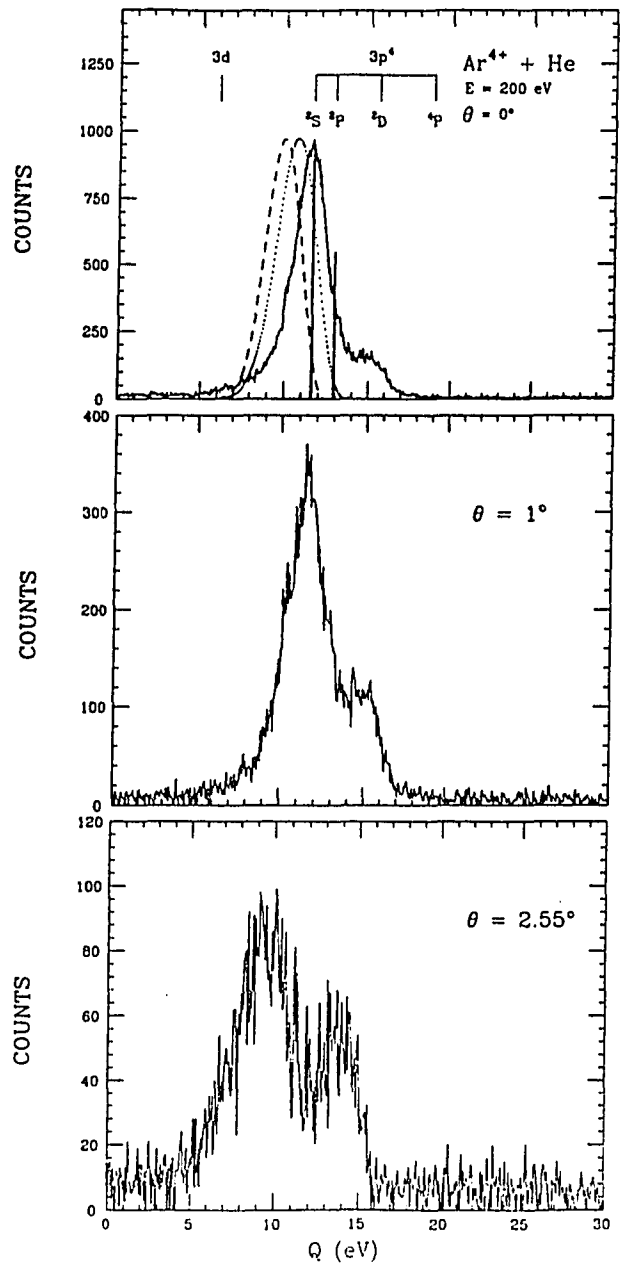

Figure 14. Translational Energy-Gain Spectra for Single-Electron Capture by 200 eV Ar^{4+} Ions From He at Different Scattering Angles.

Reaction Windows are Calculated on the Basis of a Single Crossing Landau-Zener Theory Using Values of H_{12} With Factors of 9.13 (Broken Curve) and 5.48 (Dotted Curve). The Vertical Lines Show Results of MCLZ Calculations.

dent Ar^{4+} ion beam will contain ground state $3p^2\ ^3P$ ions as well as ions in the two metastable states ^1D and ^1S which lie respectively at about 2 and 4.7 eV above the ground state. These two states contribute in varying amounts to the peak at Q ≈ 15 eV. The long tail on the lower energy side of the dominant peak (Q≤ 10 eV) is due to capture by ground state and low lying metastable incident ions into the 3d state of Ar^{3+}.

As the scattering angle is increased, single electron capture into the $3p^4\ ^2D$ of Ar^{3+} is strongly increased. This indicates that the angular distribution for capture into the $3p^4\ ^2S$ state of Ar^{3+} is strongly peaked in the forward direction in Ar^{4+} - He collisions. In greater detail, Figure 15 shows the intensity ratio $I(^2D)$ / $I(^2S)$ for capture into ^2S and ^2D states taken from the observed spectra as a function of the scattering angle. As the angle is increased, contributions from successively smaller internuclear separation regions (large Q-value) make their appearance. In addition, another particularly interesting feature of the scattering angle dependence of the electron capture spectra is that the translational energy given to the target increases as the angle increases. This feature is observed as a smaller shift in the energy-gain of the dominant peak.

The reaction windows shown in Figure 14 are based on the Kimura (1984) and the Olson and Salop (1976) expres-

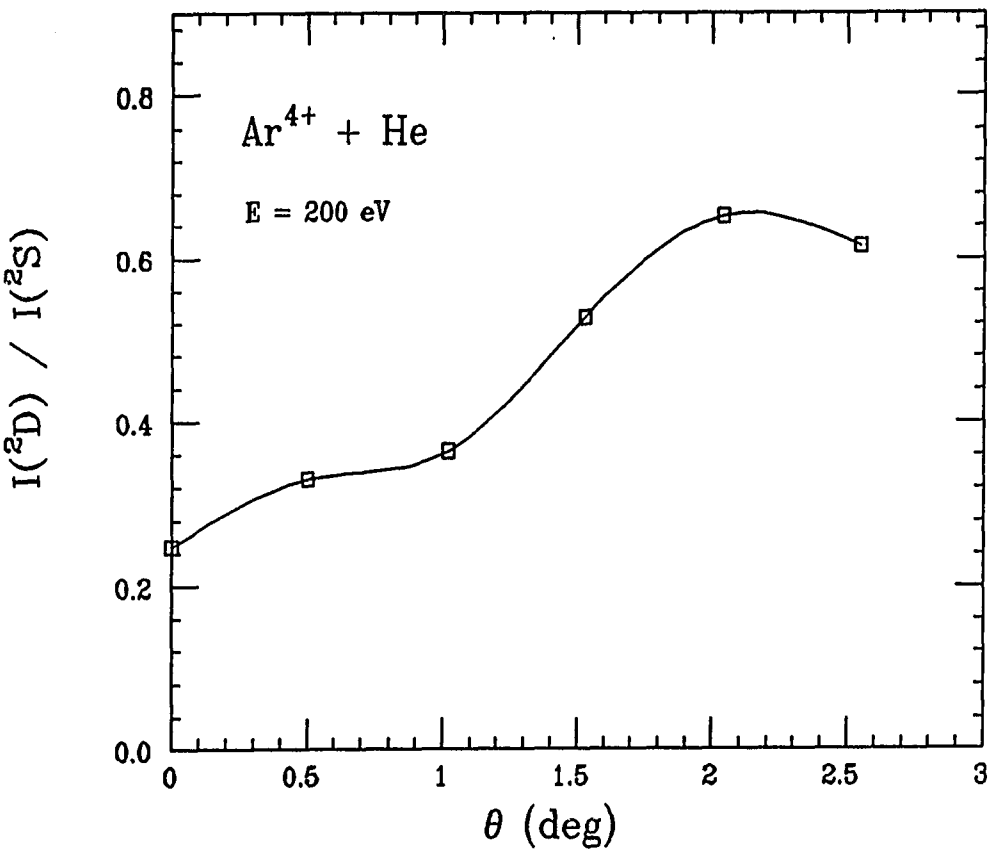

Figure 15. The Ratio $I(^2D) / I(^2S)$ as a Function of the Scattering Angle.

sions for H_{12} with factors of 5.48 and 9.13, respectively, Peak values have been normalized to the observed dominant peak value in the energy-gain spectrum. It can be seen that the reaction window based on the factor 5.48 is in better agreement with the dominant reaction channel, while the reaction window based on the factor 9.13 favors smaller energy-gain values than observed.

Also the MCLZ model has been used to calculate cross sections for single electron capture into individual channels using the probability accumulation procedure which has been discussed in detail by several authors (Giese et al., 1986; Kamber, 1988; McCullough et al., 1987). The results of these calculations using the Taulbjerg expression (Equation 2.13) for H_{12} are shown as vertical lines in the figure, with the value of largest cross section being normalized to the height of the dominant peak observed in the energy-gain spectrum. All reaction channels corresponding to ground-state Ar^{4+} ions are used in the calculations. The MCLZ calculations correctly predict the position of the dominant reaction channel and overestimate the contribution of the ^2D and ^2P reaction channels relative to the dominant reaction channel.

Ar^{4+} - Ar collisions

Typical translational energy-gain spectra showing peaks due to single-electron capture into the excited

states of the projectile product are shown in Figure 16 for 200 eV Ar^{4+} -Ar collisions for several scattering angles. Also shown are reaction windows calculated on the basis of a single crossing Landau-Zener theory using values of H_{12} containing factors 9.13 (broken curve) and 5.48 (dotted curve). The vertical lines show the MCLZ calculations. The zero-angle spectrum shows only one peak; this peak arises from single-electron capture into the 4p state of Ar^{3+} from ground state $Ar^{4+}(3p^2\ ^3P)$ (see Table 2). Other reaction channels having higher exoergicity due to capture into 4s' and 4s excited states open at scattering angles larger than 3°. These broad peaks, centered around 16 eV, are due to transfer ionization processes, presumably due to double-electron capture into autoionizing states which emit electrons before detection and thus appear to have captured only a single-electron.

Figure 17 displays the measured differential cross sections for single-electron capture by Ar^{4+} ions from Ar into the 4p state of Ar^{3+} at a collision energy of 200 eV. The data show that the distribution for capture into the 4p state is strongly peaked in the forward direction and is a smoothly decreasing function. In the transfer ionization process, however, projectile ions are scattered to larger angles compared with single-electron capture, because of the stronger Coulomb repulsion between the collision partners after the collision. It is well established that

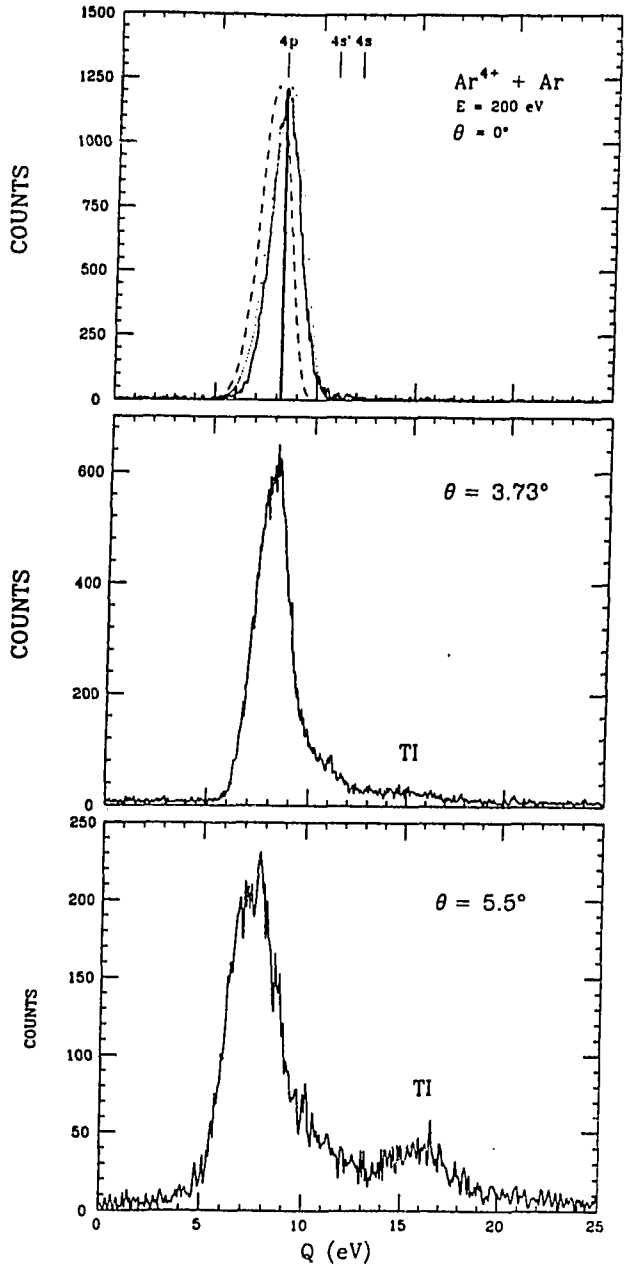

Figure 16. **Translational Energy-Gain Spectra for Single-Electron Capture by 200 eV Ar^{4+} Ions From Ar at Different Scattering Angles.**

Reaction Windows are Calculated on the Basis of a Single Crossing Landau-Zener Theory Using Values of H_{12} With Factors of 9.13 (Broken Curve) and 5.48 (Dotted Curve). The Vertical Lines Show Results of MCLZ Calculations.

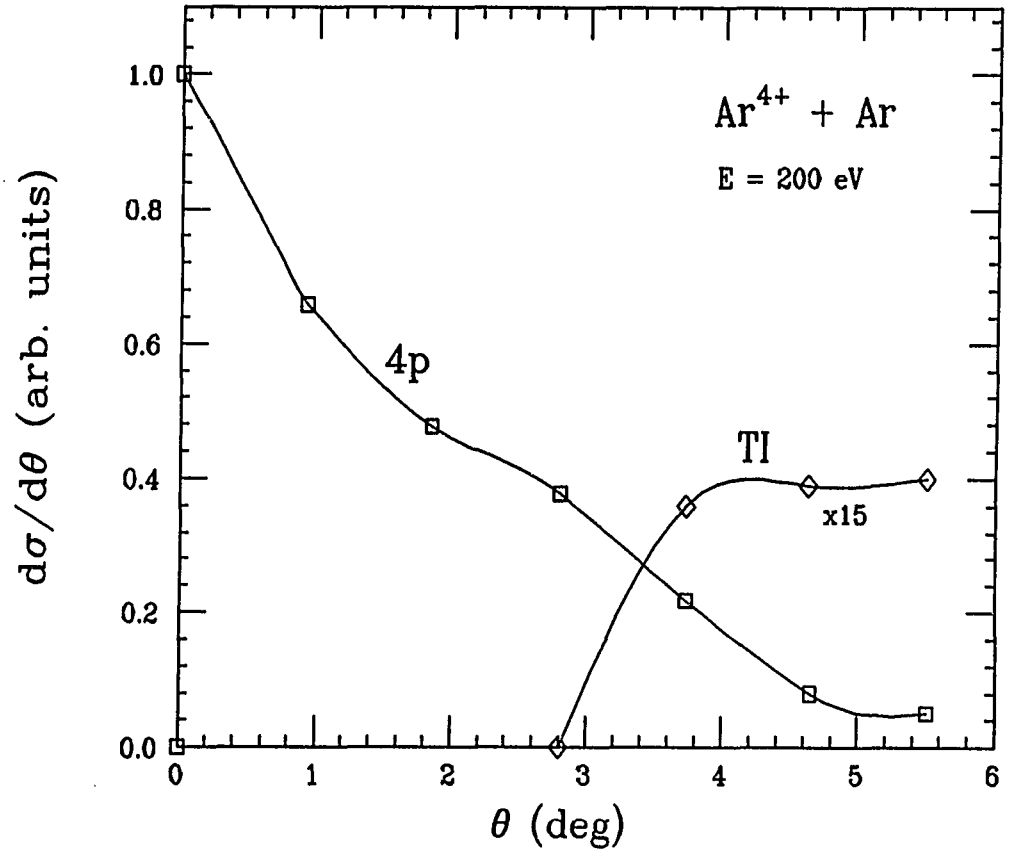

Figure 17. Differential Cross Sections for Single-Electron Capture Into the 4p State of Ar^{3+} and Transfer Ionization (TI) for 200 eV Ar^{4+} on Ar.

these transfer ionization processes are produced by a two-step mechanism. Roncin, Barat, and Laurent (1986) measured the differential cross sections for single and double-electron capture by highly-charged ions. They found that, for electrons captured simultaneously, the scattering occurs in the forward direction whereas for electrons captured successively the scattering occurs at angles greater than zero. Earlier measurements by Puerta et al. (1985) for this collision system at 800 eV impact energy show that the reaction channel due to capture into the 4p state is predominant. Their measurements also show two small peaks at 10 and 12.4 eV, which they correlate with capture into the 4s ^2P state and with the presence of metastable states in the Ar^{4+} ion beam. Comparison with the recent measurements of Biedermann et al. (1990) at 200 eV incident beam energy shows good agreement with our measurements.

For this collision system, the reaction window based on the factor 5.48 again provides the best description of the observed spectrum. Also, the MCLZ theory correctly predicts the position of the dominant reaction channel.

Ar^{5+} - He collisions

Figure 18 shows the translational energy spectra for single-electron capture by 250 eV Ar^{5+} ions from He at scattering angles of 0°, 1.53° and 3.06°. Also shown are reaction windows calculated on the basis of a single

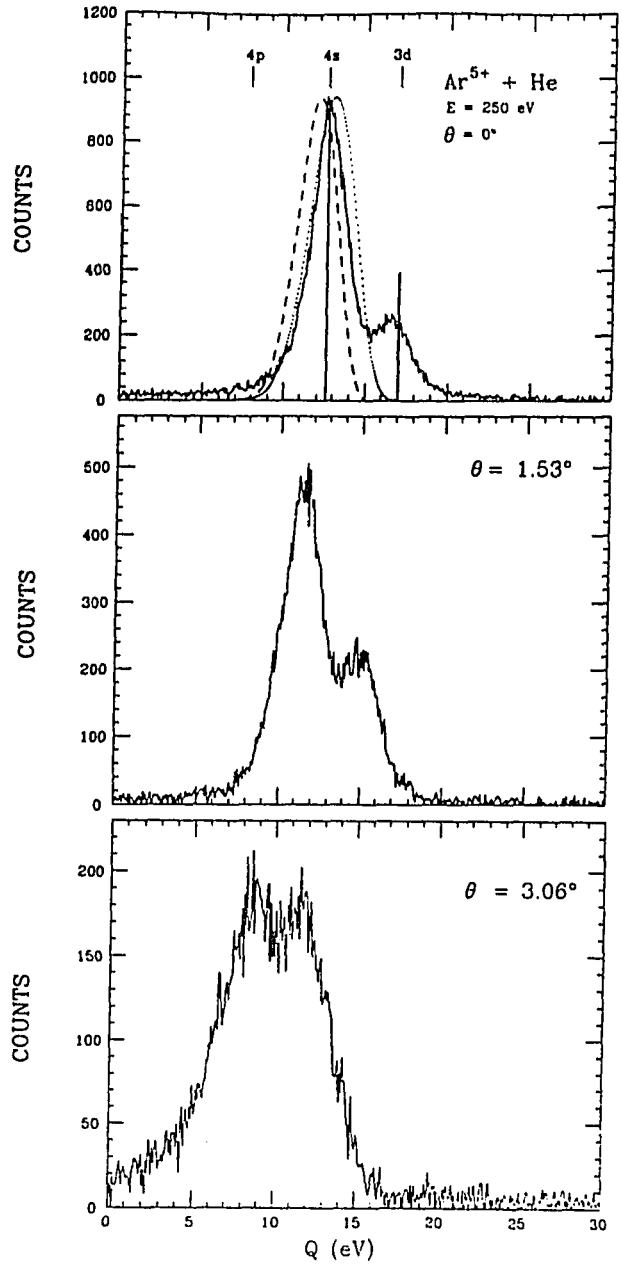

Figure 18. Translational Energy-Gain Spectra for Single-Electron Capture by 250 eV Ar^{5+} Ions From He at Different Scattering Angles.

Reaction Windows are Calculated on the Basis of a Single Crossing Landau-Zener Theory Using Values of H_{12} With Factors of 9.13 (Broken Curve) and 5.48 (Dotted Curve). The Vertical Lines Show Results of MCLZ Calculations.

crossing Landau-Zener theory using values of H_{12} for the factors 9.13 (broken curve) and 5.48 (dotted curve). The vertical lines show the MCLZ calculations. At 0° scattering angle, the dominant peak is due to capture into the 4s state of Ar^{4+} (see Table 3). There is also a significant contribution from the reaction involving capture into the 3d state. The calculated reaction window based on the factor 5.48 fits most of the observed features in the spectrum, while the MCLZ theory overestimates the contribution of the 3d capture channel. Again, a shift of about 4 eV in the energy-gain of the 4s capture channel is observed, as the scattering angle is increased from 0° to 3.06° which is attributed to the translational energy given to the target.

At each scattering angle the observed spectrum was used to determine the electron capture probabilities for the processes corresponding to capture into the 4s and 3d states. The electron capture probability is found from the ratio of the intensity of each reaction channel to the total signal. Figure 19 shows these probabilities as a function of scattering angle.

Ar^{5+} - Ar collisions

In this collision system, the observed zero-angle spectrum at an impact energy of 250 eV shows that capture into the ($3s^2$ 3p 4d) state dominates, while capture into the

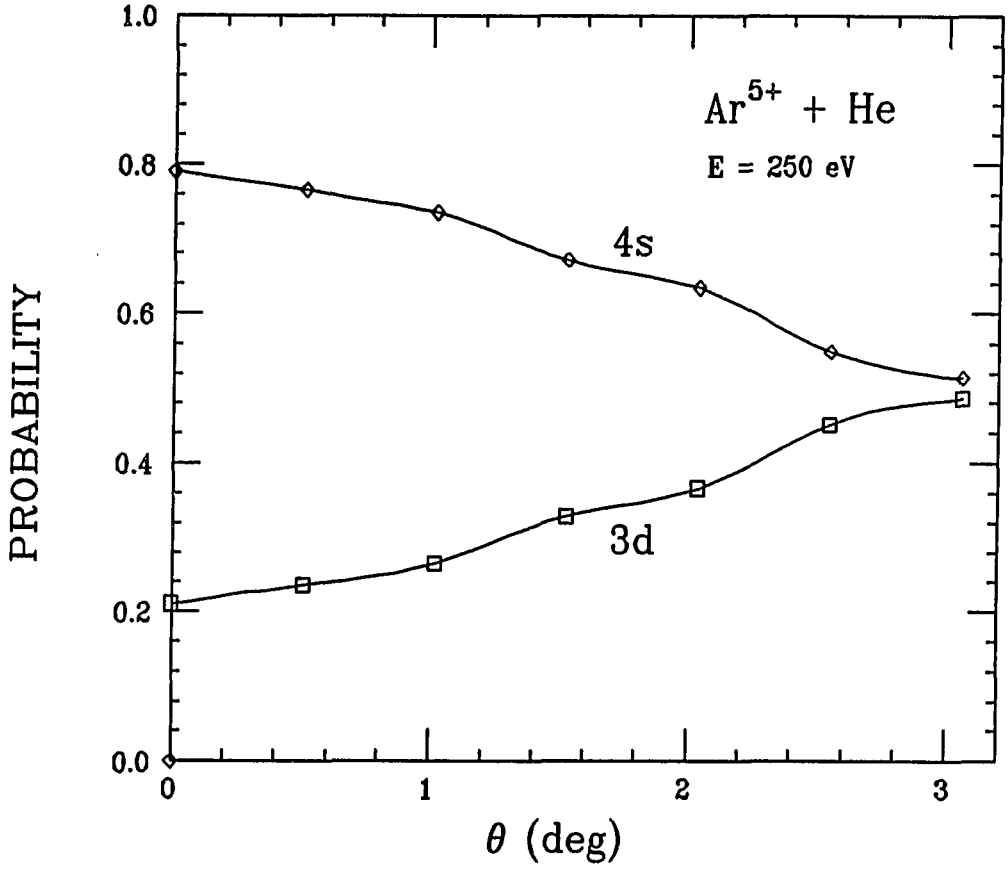

Figure 19. Probability of Single-Electron Capture as a Function of Scattering Angle for 250 eV Ar^{5+} - He Collisions.

($3s^2$ 3p 4p) state shows less contribution (see Figure 20 and Table 4). The electron capture probabilities for the reaction channels corresponding to capture into 4p and 4d states of the Ar^{4+} ions and transfer ionization processes produced in Ar^{5+} - Ar collisions are displayed in Figure 21. Three features are emphasized:

1. The 4d state of Ar^{4+} produced in the electron capture process is strongly forward scattered. This behavior corresponds to a large impact parameter mechanism.

2. The reaction channel due to capture into the 4p state of Ar^{4+} is significantly populated in the collision process and becomes comparable to capture into the 4d state for scattering angles near 3°.

3. The contribution of transfer ionization strongly increases with increasing scattering angle.

The calculated reaction window using the factor 5.48 generally fits most of the observed spectrum. For this collision system, the MCLZ theory predicts relative cross sections which are in good agreement with the measurements.

Giese et al. (1986) have studied the Ar^{5+} - Ar system at a collision energy of 2725 eV. They found that the reaction channel correlating with capture into the 4p state produced almost the same contribution as did the reaction channel due to capture into the 4d state. This is attributed to the high impact energy they used since the position of the reaction window, which indicates the favored final

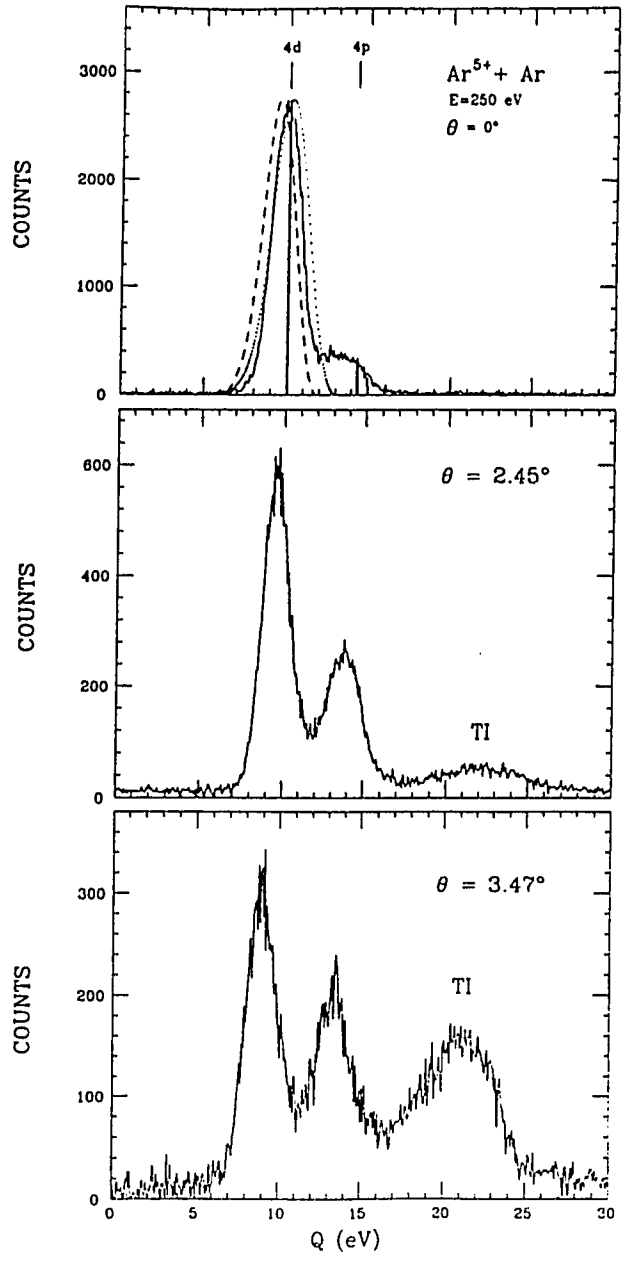

Figure 20. Translational Energy-Gain Spectra for Single-Electron Capture by 250 eV Ar^{5+} Ions From Ar at Different Scattering Angles.

Reaction Windows are Calculated on the Basis of a Single Crossing Landau-Zener Theory Using Values of H_{12} With Factors of 9.13 (Broken Curve) and 5.48 (Dotted Curve). The Vertical Lines Show Results of MCLZ Calculations.

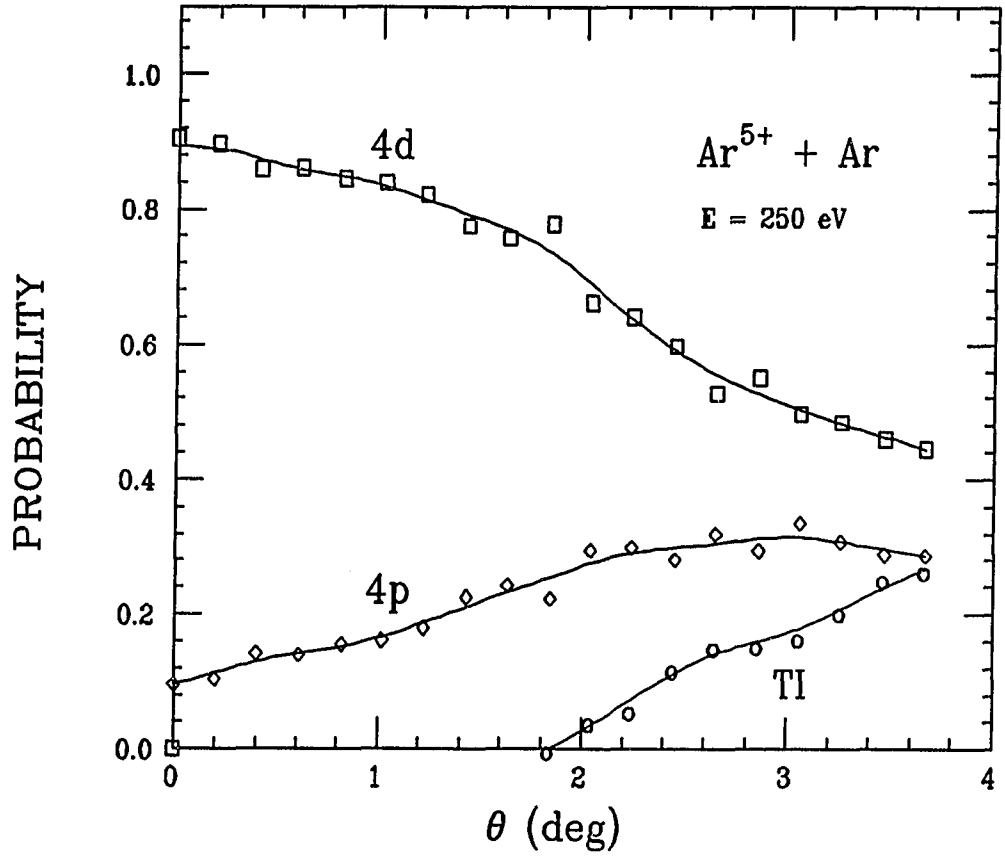

Figure 21. Probability of Single-Electron Capture as a Function of Scattering Angle for 250 eV Ar^{5+} - Ar Collisions. TI Denotes Transfer Ionization.

states, depends mainly on the collision energy of the projectile. When the collision energy is reduced the adiabaticity of inner crossings becomes increasingly pronounced, while the transition probability at distant crossings becomes larger. Therefore, the reaction window shifts towards larger internuclear separations if the collision energy is reduced and vice versa.

The variation of the translational energy spectra for single-electron processes is plotted as a function of collision energy for the Ar^{5+} - Ar collision system in Figure 22. The relative cross sections for capture into the 4d and 4p states of Ar^{5+} become of comparable importance at 500 eV with the cross section ratio $\sigma(4p)$ / $\sigma(4d)$ increasing with increasing collision energy from 0.08 at 125 eV to 0.375 at 500 eV.

Kinematic Effects

Calculated kinematics for reaction channels 4s and 3d in Ar^{5+} - He, and 4d and 4p in Ar^{5+} - Ar collisions are shown in Figure 23. It is interesting to note that at large projectile scattering angles the translational energy of the recoil target ions (small Q values) becomes very important for Ar^{5+} - He and not so important for Ar^{5+} - Ar collisions.

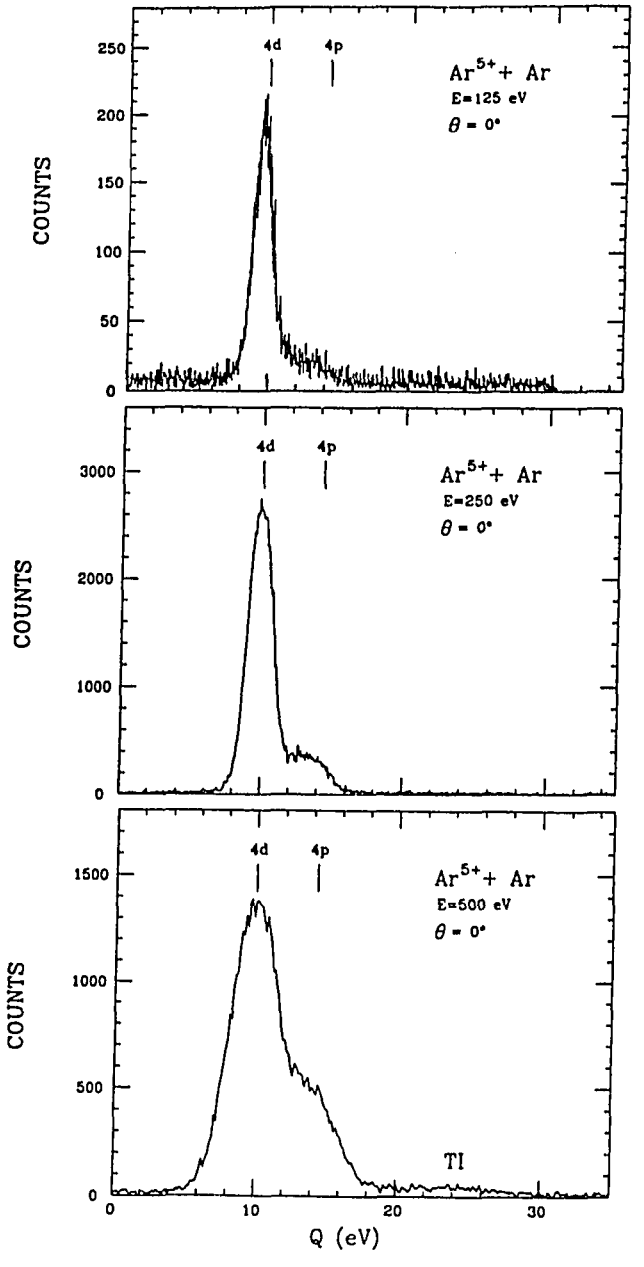

Figure 22. Translational Energy-Gain Spectra for Single-Electron Capture by Ar^{5+} Ions From Ar at Various Collision Energies.

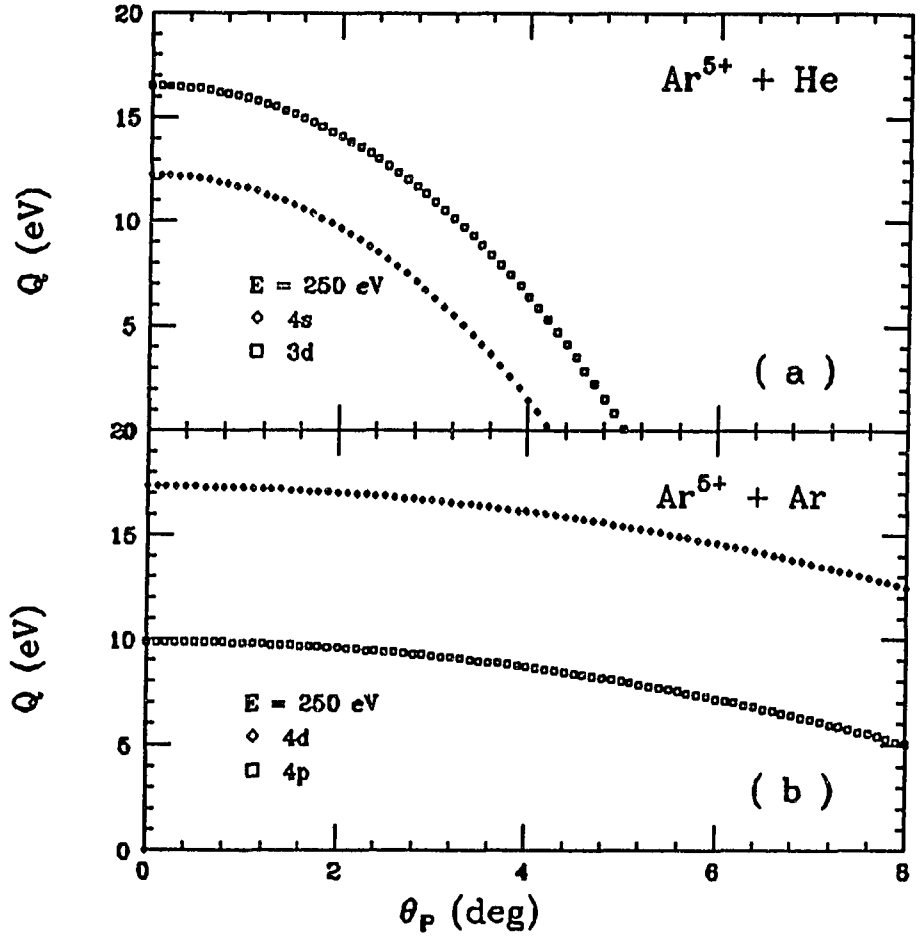

Figure 23. (a) Calculated Energy-Gain (Q) Values of (4s) and (3d) Versus Projectile Scattering Angle θ_p for Ar^{5+} - He.
(b) Calculated Energy-Gain (Q) Values of (4d) and (4p) Versus Projectile Scattering Angle θ_p for Ar^{5+} - Ar.

CBM Model

The classical over barrier transition model (CBM) predicts that the exit channel with the largest possible principal quantum number n, satisfying the condition $n \leq n_{cmb}$, should be dominantly populated. This is equivalent to taking the exit channel with the largest possible crossing radius R_x satisfying $R_x \leq R_{cmb}$. Values of n, R_x, n_{cmb} and R_{cmb} are given in Table 5 for the four collision systems investigated. Inspection of the experimental results shows that the predictions of this model are incorrect for all systems studied. The measured R_x (Dalgarno & Butler, 1978)

$$R_x(au) = 27.2(q-1)/\Delta E(eV) \qquad (5.1)$$

neglecting polarization, for all the dominant reaction channels are always larger than the R_{cbm} values. However, the model does correctly predict which n shell is predominantly populated for Ar^{4+} - He and Ar^{5+} - Ar collisions systems.

Table 5

Summary of Measured Collision Parameters for Single-Electron Capture Processes Compared With Classical Over Barrier Model

Collision System	n_{cmb}[1]	R_{cmb}[2](au)	n	R_x(au)
Ar^{4+} - He	2.4	5.5	3	6.5
Ar^{4+} - Ar	2.9	8.6	4	9.6
Ar^{5+} - He	2.8	6.0	4	8.5
Ar^{5+} - Ar	3.5	9.4	4	10.9

[1]From Equation (2.21).
[2]From Equation (2.20).

CHAPTER VI

CONCLUSION

The main purpose of this thesis was to investigate state-selective differential cross sections for single-electron capture by low-energy Ar^{4+} and Ar^{5+} ions from He and Ar by means of translational energy-gain spectroscopy. Measurements were carried out at the laboratory impact energies of 25q, 50q, and 100q eV (q = 4 and 5, where q is the ion charge state) and at laboratory scattering angles between 0° and 5.5°.

The translational energy-gain spectra show only a few final states were populated. The transition probabilities depend strongly on the charge state of the projectile ion and the ionization potential of the target atom, and only weakly on the impact energy. The reaction window obtained from the Landau-Zener theory using the factor 5.48 provides the best general description of the observed features. The MCLZ calculations correctly predict the positions of the dominant reaction channels that are observed and are in qualitative agreement with the magnitude of the measured cross sections.

Additionally the measurements demonstrate the importance of dynamic effects in the single-electron capture

process. In particular, they reveal an interesting impact-parameter dependence of electron capture; as the angle is increased, contributions from successively smaller internuclear separations (larger Q-values) become significant as expected.

BIBLIOGRAPHY

Afrosimov, V. V., Basalaev, A. A., Panov, M. N., & Samoilov, A. V. (1986). Electron capture from helium atoms into various electronic states by multiply charged argon ions. Soviet Physics JETP, 64, 273.

Arianer, J., & Geller, R. (1981). The advanced positive heavy ion source. Annual Review of Nuclear and Particle Science, 31, 19.

Bashkin, S., & Stoner, J. O. (1978). Atomic energy levels and Grotrian Diagrams. Amsterdam: North-Holland.

Biedermann, C., Cederquist, H., Andersson, L. R., Levin, J. C., Short, R. T., Elston, S. B., Gibbons J. P., Anderson, H., Liljeby, L., & Sellin, I. A. (1990). Experimental and model angular distributions of one- and two-electron capture processes in 0.5 - 20 Ev/u Ar^{4+} - Ar collisions. Physical Review A, 41, 5889.

Butler, S. E., Heil, T. G., & Dalgarno, A. (1980). Charge transfer of multiply charged ions with hydrogen and helium: Quantal calculations. The Astrophysical Journal, 241, 442.

Cederquist, H., Liljeby, L., Biedermann, C., Levin, J. C., Rothard, H., Groeneveld, K. O., Vane, C. R., & Sellin, I. A. (1989). State selected angular distributions of single electron capture in very slow Ar^{4+} - Ar collisions. Physical Review A39, 8, 4308.

Cooks, R. G. (1978). Collision spectroscopy. New York: Plenum Press.

Dalgarno, A. (1985). Charge transfer processes in astrophysical plasmas. Nuclear Instruments and Methods in Physics Research, B9, 655.

Dalgarno, A., & Butler, S. E. (1978). Charge transfer of multiply-ionized species. Comments Atomics Molecular Physics, 7, 129.

Ferguson, S. M. (1992). Private communication.

Giese, J. P., Cocke, C. L., Waggoner, W. T., Pedersen, J.

O. K., Kamber, E. Y., & Tunnell, L. N. (1987). Non-Franck-Condon transitions in two-electron capture from D_2 by low-energy, highly charged Ar projectiles. Physical Review A38, 9, 4494.

Giese, J. P., Cocke, C. L., Waggoner, W. T., & Tunnell, L. N. (1986). Energy-gain spectroscopy of electron-capture collisions between low-energy Ar and Ne projectiles and atomic and molecular deuterium targets. Physical Review A, 34, 3770.

Hansen, J. P., & Taulbjerg, K. (1988). Electron capture in highly charged ion collisions and a theoretical analysis of the energy-gain spectrum. Journal of Physics B, 21, 2459.

Janev, R. K., & Winter, H. (1985). State-selective electron capture in atom-highly charged ion collisions. Physics Reports, 117, 265.

Kamber, E. Y. (1988). State-selective single- and double-electron capture by Ar^{4+} and Ar^{5+} ions from rare-gas atoms. Journal of Physics B, 21, 4185.

Kamber, E.Y. (1989). Electron capture into excited states by Ar^{5+} ions from He and Ne. Nuclear Instruments and Methods in Physics Research B, 40/41, 13.

Kamber, E. Y., Cocke, C. L., Giese, J. P., Pedersen, J. O. K., & Waggoner, W. (1987). State-selective differential single-electron capture cross sections for O^{2+} - He collisions. Physical Rewiev A, 36, 5575.

Kamber, E. Y., Cocke, C. L., Giese, J. P., Pedersen, J. O. K., Waggoner, W., & Varghese, S. L. (1987). An experimental apparatus for studying double differential scattering by low energy X^{q+} ions from He. Nuclear Instruments and Methods in Physics Research B, 24/25, 288.

Kimura, M., Iwai, T., Kobayashi, N., Matsumoto, A., Ohtani, S., Okuno, K., Takagi, S., Tawara, H., & Tsurubuchi, S. (1984). Landau-Zener model calculations of one electron capture from He atoms by highly stripped ions at low energies. Journal of Physical Society of Japan 53, 7, 2224.

Landau, L. D. (1932). Energy calculations of diabatic crossings. Physics Z. Soviet Union, 2, 46.

Louisell, W. H., Scully, O. M., & McKnight, W. B. (1975).

Analysis of a soft-x-ray laser with charge-exchange excitation. Physical Review A, 11, 989.

Mann, R., Folkmann, F., & Beyer, H. F. (1981). Selective electron capture into highly stripped Ne and N target atoms after heavy-ion impact. Journal of Physics B, 14, 1161.

McCullough, R. W., Wilson, S. M., & Gilbody, H. B. (1986). State-selective capture by slow Ar^{4+}, Ar^{5+} and Ar^{6+} recoils ions in H, H_2 and He. Journal of Physics B, 20, 2031.

Meyer, F. W., Howald, A. M., Havener, C. C., & Phaneuf, R. A. (1985). Observation of low-energy Z oscillations in total electron capture cross sections for bare projectiles colliding with H and H_2. Physical Review Letters 54, 25, 2663.

Miller, B., Could, R. W., Frieman, E. A., & Triuelpiece, A. W. (1974). Charge transfer calculations for a plasma. Review of research programs of the division of controlled thermo nuclear research, ERDA-39 (Energy Research and Development Administration), Washington DC, 145.

Niehaus, A. (1986). A classical model for multiple-electron capture in slow collisions of highly charged ions with atoms. Journal of Physics B, 19, 2925.

Nielsen, E. H., Andersen, L. H., Barany, A., Cederquist, H., Heinnemeir, J., Hvelplund, P., Knudsen, H., MacAdam, K. B., & Sorensen, J. (1985). Energy gain spectroscopy of state selective electron capture for multiply charged Ar recoil ions. Journal of Physics B, 18, 1789.

Olson, R. E., & Kimura, M. (1982). Angular scattering in slow multiply-charged ion, atom collisions. Journal of Physics B, 15, 4231.

Olson, R.E., & Salop, A. (1976). Electron transfer between multicharged ions and neutral species. Physical Review A, 14, 579.

Pequignot, D. (1980). Charge transfer reactions in some astrophysical situations. Astronomy Astrophysics 81, 3, 356.

Puerta, J., Kahlert, H. J., Koslowski, H. R. & Huber, B. A. (1985). Nuclear Instrumental Methods B, 9, 415.

Roncin, P., Barat, M., & Laurent, M. (1986). Differential cross-sections for one- and two-electron capture by highly charged ions (N^{7+}, O^{7+}, O^{8+}, Ne^{7+}, Ne^{8+}) at low keV energies. Europhysics Letters, 2, 371.

Ryufuku, H., Sasaki, K., & Watanabe, T. (1980). Oscillatory behavior of charge transfer cross sections as a function of the charge of projectiles in low-energy collisions. Physical Review A, 21, 745.

Salop, A., & Olson, R. E. (1975). Charge exchange between H(1s) and fully stripped heavy ions at low-keV impact energies. Physical Review A, 13, 1312.

Stueckelberg, E. C. G. (1932). Theory of the inelastic collision between the atoms. Helvetica Physica Acta, 5, 369.

Taulbjerg, K. (1986). Reaction windows for electron capture by highly charged ions. Journal of Physics B, 19, L367.

Zener, C. (1932). Non-Adiabatic crossing of energy levels. Progress in Royal Society London A, 137, 696.